

**Radiation Effects on the Sorption and Mobilization of Radionuclides  
during Transport through the Geosphere — Final Technical Report**

(Award number: DE-FG07-97ER45652)

L.M. Wang<sup>a,b</sup>, R.C. Ewing<sup>a,b,c</sup> and K.F. Hayes<sup>d</sup>

<sup>a</sup>Department of Nuclear Engineering and Radiological Sciences

<sup>b</sup>Department of Materials Science and Engineering

<sup>c</sup>Department of Geological Sciences

<sup>d</sup>Department of Civil and Environmental Engineering

The University of Michigan, Ann Arbor, MI 48109

March 14, 2004

Principal Investigator contact information:

Dr. Lumin Wang

Department of Nuclear Engineering and Radiological Sciences

The University of Michigan, Ann Arbor, MI 48109-2104

(734) 647-8530 (phone)

(734) 647-8531 (fax)

[lmwang@umich.edu](mailto:lmwang@umich.edu) (e-mail)

## **TABLE OF CONTENTS**

<b>COVER PAGE.....</b>	<b>1</b>
<b>TABLE OF CONTENTS.....</b>	<b>2</b>
<b>SUMMARY.....</b>	<b>3</b>
<b>BACKGROUND AND SIGNIFICANCE TO EMSP.....</b>	<b>5</b>
<b>RESEARCH ACCOMPLISHMENT.....</b>	<b>6</b>
<b>Previous results.....</b>	<b>5</b>
<b>Research progress during 2001-2003 .....</b>	<b>10</b>
<b>1. Neutron irradiation of zeolites .....</b>	<b>10</b>
<b>2. Proton irradiation of zeolites .....</b>	<b>21</b>
<b>3. Thermal effects on zeolites.....</b>	<b>27</b>
<b>4. Thermal effects on the Sr sorption on clay.....</b>	<b>33</b>
<b>Publications and invited talks.....</b>	<b>36</b>
<b>REFERENCES.....</b>	<b>39</b>
<b>PROPOSED FUTURE RESEARCH.....</b>	<b>41</b>

## SUMMARY

Site restoration activities at DOE facilities and the permanent disposal of nuclear waste inevitably involve understanding the behavior of materials in a radiation field. Radionuclide decay and the associated radiation fields lead to physical and chemical changes that can degrade or enhance important material properties. Alpha-decay of the actinide elements and beta-decay of the fission products lead to atomic-scale changes in materials (radiation damage and transmutation). The radiation exposure due to the release and sorption of long-lived actinides and fission products (e.g.,  $^{137}\text{Cs}$  and  $^{90}\text{Sr}$ ) may cause changes in important transport properties (e.g., sorption and cation exchange capacity) in geological materials, such as colloidal clays and zeolites, along transport pathways. Thus, the effect of radioactive decay on soils and geologic materials during transport (e.g., through the vadose zone) are an important aspect of understanding the migration and retention of radionuclides in the geosphere.

During the previous funding period of this project, we have evaluated radiation effects in selected near-field materials with accelerated laboratory experiments utilizing energetic electrons and ions and *in situ* transmission electron microscopy (TEM) during irradiation at the HVEM/IVEM-Tandem National Facility at Argonne National Laboratory. The materials irradiated included zeolites and layered silicates (mica and clays). We have found that all of these materials are susceptible to irradiation-induced solid-state amorphization. Amorphization can either be induced by ionization processes ( $\beta$ - or  $\gamma$ - irradiation) or by direct displacement damage processes ( $\alpha$ -decay events). The critical doses for complete amorphization of these phases are as low as  $<0.1$  displacement per atoms (dpa) or  $10^8$  Gy in ionization energy deposition (a dose expected in a zeolite with 10 wt.% loading of  $^{137}\text{Cs}$  in 400 years). Experiments on thermally-induced amorphization have shown that even partial amorphization will cause a dramatic reduction (up to 95%) in ion-exchange and sorption/desorption capacities for radionuclides, such as Cs and Sr. Because the near-field or chemical processing materials, e.g., zeolites or crystalline silicotitanate (CST), will receive a substantial radiation dose after they have incorporated radionuclides, our results suggest that radiation effects may, in some cases, retard the release rate of sorbed or ion-exchanged radionuclides. **These results have a direct bearing on repository performance assessments (e.g., the extent to which zeolites can retard the release of radionuclides) and on the technologies used to process high-level liquid wastes (e.g., separation of  $^{137}\text{Cs}$  from HLW using CST at the Savannah River Site).** Because the dose rate of available gamma sources is too low to achieve significant effects in a reasonable period (e.g., requires 50 years to reach the critical amorphization dose for zeolite-NaY), heavy ions or energetic electrons in an electron microscope were used in our previous studies.

Although these experiments are adequate for studying the radiation effects on the microstructure of the target material, the radiation affected volume is too small for studying changes in bulk properties, such as sorptive or ion-exchange capacities of clays and zeolites which is of critical importance because these phases play an important role in the retardation of radionuclides in the geosphere.

During the last two years, we have continued our study of radiation effects on the sorption and ion-exchange capacities of two important groups of materials: clays and zeolites with newly designed experimental methods (proton and neutron irradiation). These newly designed experiments generated much larger quantity of damaged materials for the ion exchange and leaching tests as well as for detailed structural and microstructural studies. Cross-sectional analytical electron microscopy on proton irradiated zeolite samples with or without Cs or Sr loading has shown similar results as previously observed in thermally amorphized samples. Twenty four zeolite samples have been irradiated in the Ford Nuclear Reactor with thermal neutrons in eight batches. One third of the samples were preloaded with Sr and another one third was preloaded with Cs. These nuclides are important because: 1.) they represent a range of sorptive behavior that should bracket the behavior of most other radionuclides and 2.) they are considered to make important contributions to total radiation exposures, as illustrated in the Total Systems Performance Assessment-Viability Assessment of the proposed repository at Yucca Mountain. Ion exchange/sorption experiments are being conducted for samples irradiated to various doses to determine the impact of the radiation effects on the sorption capacity and retention of radionuclides. The irradiated material are also being characterized by a wide variety of analytical techniques (e.g., x-ray diffraction, X-ray absorption spectroscopy, and X-ray absorption spectroscopy) to precisely describe the nature of the radiation damage at the near atomic-scale. These analysis combined with the sorption and cation-exchange results are providing important information for determining the relationships among key parameters: radiation damage dose, microstructure at the surface, materials properties (e.g., aperture size of the zeolites), and radionuclide sorption and/or ion exchange.

## **BACKGROUND AND SIGNIFICANCE TO EMSP**

Site restoration activities at DOE facilities and the permanent disposal of nuclear waste generated at DOE facilities involve working with and within various types and levels of radiation fields. Radionuclide decay and the associated radiation fields lead to physical and chemical changes that can degrade or enhance material properties. The principal sources of radiation at the DOE sites are the actinides and fission-products contained in high-level wastes currently in storage. Alpha-decay of the actinide elements and beta-decay of the fission products lead to atomic scale changes in the material (radiation damage and transmutation) (Ewing et al., 1995; Ewing, 1999; Weber et al., 1997, 1998). During site restoration, materials will be exposed to radiation fields that exceed  $10^4$  rad/hr. The radiation exposure due to the release and sorption of long-lived actinides (e.g.,  $^{237}\text{Np}$ ) and fission products (e.g.,  $^{137}\text{Cs}$  and  $^{90}\text{Sr}$ ) may cause changes in important properties (e.g., cation exchange capacity) in geological materials (e.g., clays and zeolites) along transport pathways. Among these materials, clays and zeolites, which are expected to sorb and immobilize radionuclides, are known to be extremely susceptible to radiation-induced structure changes (e.g., bubble formation and solid state amorphization) through both collisional displacement and ionization processes. These changes will inevitably affect (either negatively or positively) the further sorption and the migration of radionuclides at waste sites (e.g., vadose zone at Hanford). Current models used for the long term prediction of radionuclide transport have proven to be inadequate and unrealistic; however, these previous models did not take radiation effects into consideration.

This research program has been aimed at the understanding radiation effects on the sorption/desorption and ion exchange capacity of radionuclides in two major groups of geologic materials, clays and zeolites. The proposed experiments will first investigate the effects of ionizing and particle irradiation on the zeolites and clays. We have focused on changes in the ion exchange capacity of radionuclides (e.g., Cs, Sr), and changes in the retention capacity of already incorporated radionuclides after the sample is damaged by radiation. Through a comprehensive study of the microstructure and ion exchange capacity under varying types of irradiation (collision versus ionization), dose rate, temperature and ion exchange conditions, we will develop a first principles understanding of radiation effects on the ion exchange and retention capacity of clays and zeolites. The results provide essential database for a basic understanding the long term effectiveness of clays and zeolite in radionuclide retention, as well as the mobility of the radionuclides in contaminated sites. These results will form the scientific basis for the development of both better models for the prediction of the long term migration of radionuclides and better techniques for the effective confinement of radionuclides at the DOE sites.

## RESEARCH ACCOMPLISHMENT

### Previous results

During our previous studies (1997-2000), radiation effects on the microstructures of layered silicates (micas) and zeolites have been investigated by electron microscopy after electron and ion beam irradiations. The results have shown that these materials are extremely susceptible to irradiation-induced solid-state amorphization (i.e., the materials' unique sheet or porous crystalline structure is completely destroyed by irradiation). Amorphization can either be induced by ionization processes (as occurs with  $\beta$ - or  $\gamma$ -irradiation) or by direct displacement damage processes (as by  $\alpha$ -recoils). The critical doses for complete amorphization of these phases can be as low as  $<0.1$  displacement per atom (dpa) or  $10^8$  Gy in ionization energy deposition (a dose equivalent to that expected in a zeolite with 10 wt.% loading of  $^{137}\text{Cs}$  in 400 years) (Wang, Wang, Gong and Ewing, 1998; Wang, Wang and Ewing, 1998; Wang and Weber, 1999). The progressive process of amorphization of these materials under electron irradiation is clearly demonstrated by electron diffraction (Figure 1) and by high resolution transmission electron microscopy (HRTEM) (Figure 2).

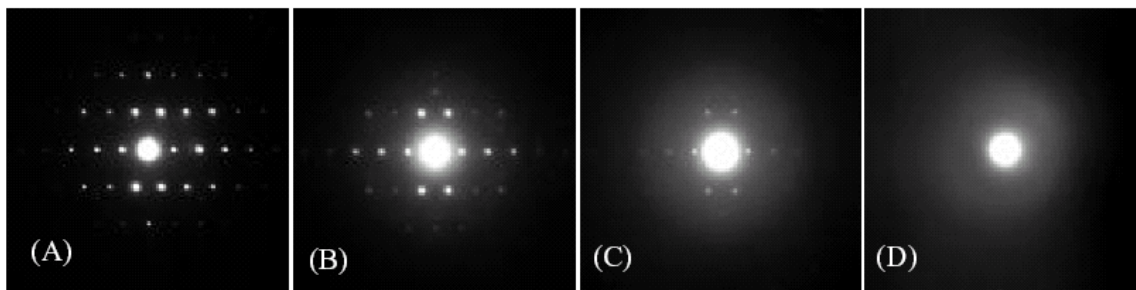


Fig. 1 Electron diffraction patterns showing the progressive changes of zeolite-Y structure from crystalline-to-amorphous under 200 keV electron irradiation at the room temperature. (A) beginning of the irradiation, (B)  $2 \times 10^{20} \text{ e}^-/\text{cm}^2$ , (C)  $3.5 \times 10^{20} \text{ e}^-/\text{cm}^2$ , and (D)  $3.4 \times 10^{20} \text{ e}^-/\text{cm}^2$  ( $1.6 \times 10^{11} \text{ Gy}$ ).

The critical amorphization dose for several sheet silicates (e.g., mica) increased with the increasing temperature due to the increased efficiency of structural recovery at elevated temperatures (Figure 3). However, in the case of zeolites and some layer silicates, radiation-induced amorphization is significantly enhanced at higher temperatures (Figure 4). Amorphization of zeolites or layered silicates may be preceded or accompanied by dehydration, layer spacing reduction and gas bubble formation (Figure 5) which may cause significant volume swelling. The critical radiation dose for amorphization or bubble formation in zeolites strongly depends on the size of channels available in the structure for gas release (Wang, Wang and Ewing, 2000). The amorphization of the crystal structure and the formation of bubbles will inevitably change the ion exchange and retention capacity of these materials for radionuclides due to the disruption of the structure or by blocking access to exchangeable cation sites. However, due to the small volumes affected by the ion or electron beam irradiations, it is difficult to conduct the ion exchange experiments with these radiation-damaged materials. Although  $\gamma$ -irradiation can affect larger volumes of the samples, available sources of  $\gamma$ -irradiation

cannot generate the extent of damage predicted for the long term effects in a reasonable experimental time frame, partly because  $\gamma$ -irradiation only causes ionizing damage and cannot reproduce the displacement damage caused by direct collision, as in  $\alpha$ -decay of actinides. Estimates based on the flux of the currently available  $^{60}\text{Co}$   $\gamma$ -source and the results of the electron irradiation experiment have indicated that more than 50 years would be needed in order to totally amorphize zeolites by  $\gamma$ -irradiation.

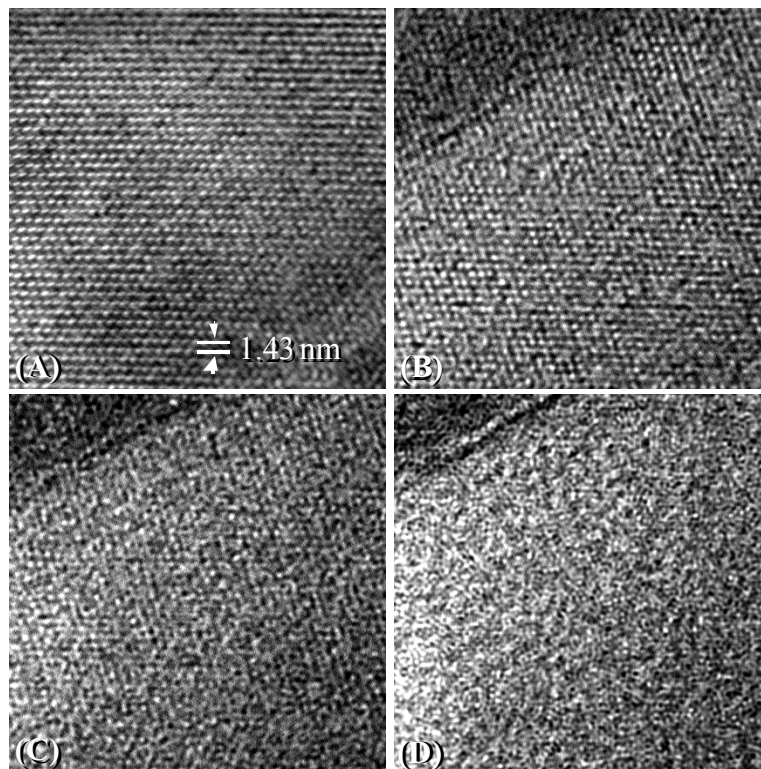


Fig. 2 HRTEM images of zeolite-Y showing the uniform and progressive change from the crystalline-to-amorphous state under a 400 keV electron irradiation at the room temperature. (A) beginning of the irradiation, (B)  $2 \times 10^{20} \text{ e}^-/\text{cm}^2$ , (C)  $4 \times 10^{20} \text{ e}^-/\text{cm}^2$ , and (D)  $6 \times 10^{20} \text{ e}^-/\text{cm}^2$ .

Because zeolites are thermally unstable and can be amorphized by thermal annealing, we have compared the ion exchange and retention capacity for Cs in zeolites before and after thermally-induced amorphization (Gu, Wang and Ewing, 2000). In this study, zeolite-NaY samples with or without Cs loading were first amorphized by thermal annealing at 900-1000°C, and then subjected to ion exchange and desorption experiments. The amorphized zeolite-NaY lost nearly 95% of its ion exchange capacity for Cs due to the loss of exchangeable cation species and/or the blockage of access to exchangeable cation sites (Figure 6). Also, the desorption study indicated that amorphization of Cs-loaded zeolite may enhance the retention capacity of exchanged Cs due to the closure of the channels (Figure 7). Because the near-field or chemical processing materials (e.g., zeolites or CST) will receive a substantial radiation dose after they have incorporated radionuclides, our results suggest that radiation-induced amorphization may, in some cases, retard the release rate of sorbed or ion-exchanged radionuclides due to the closure of internal channels. The results of these studies have a

direct bearing on repository performance assessment (e.g., the extend to which zeolites can retard the release of radionuclides) and on the technologies used to process high-level liquid wastes (e.g., separation of  $^{137}\text{Cs}$  from HLW using CST at the Savannah River Site).

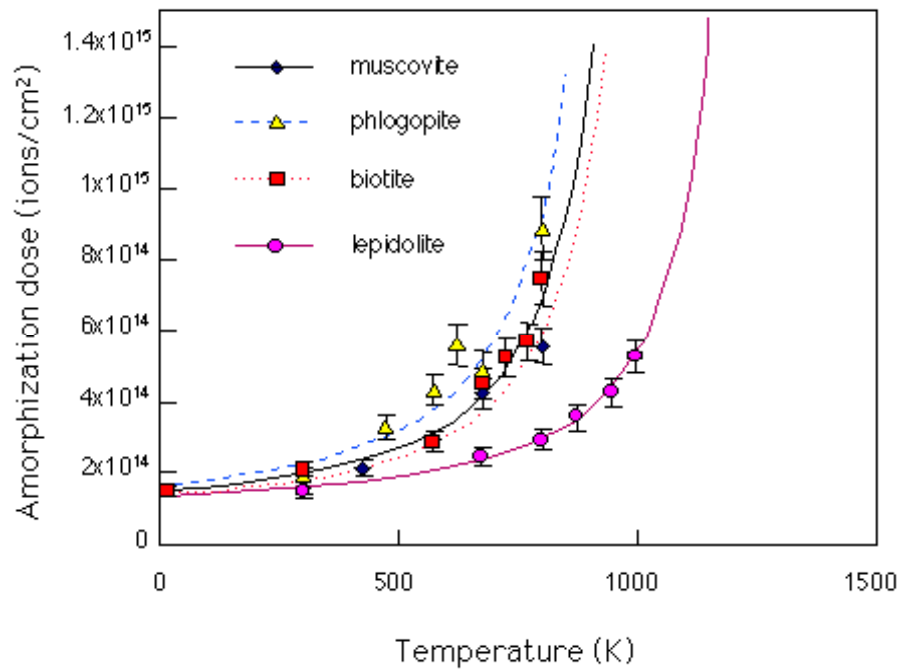


Fig. 3 Temperature dependence of critical amorphization dose of four sheet silicates under 1.5 MeV  $\text{Kr}^+$  irradiation.

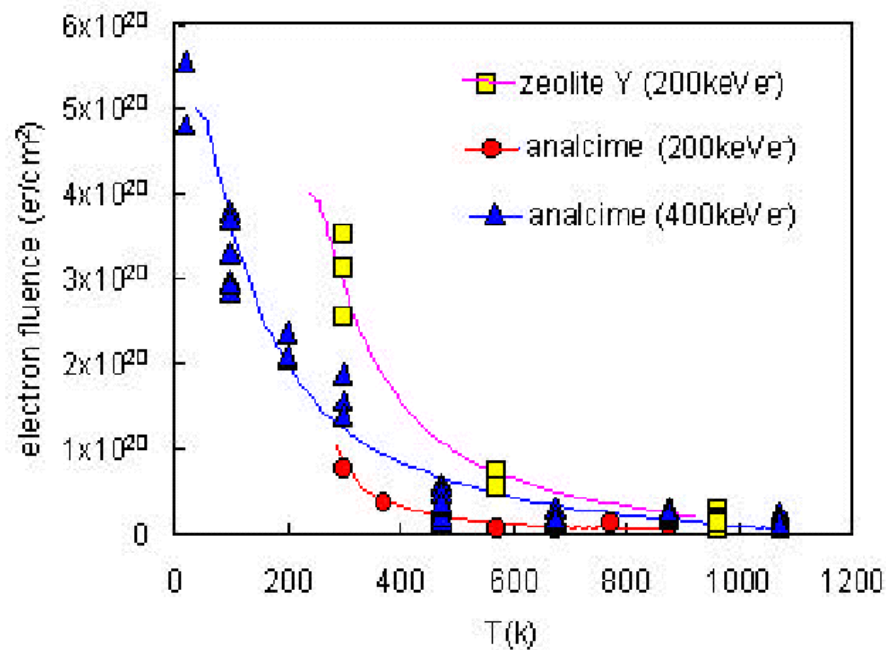


Fig. 4 Temperature dependence of amorphization dose of zeolite under 200 and 400 KeV electron irradiation.



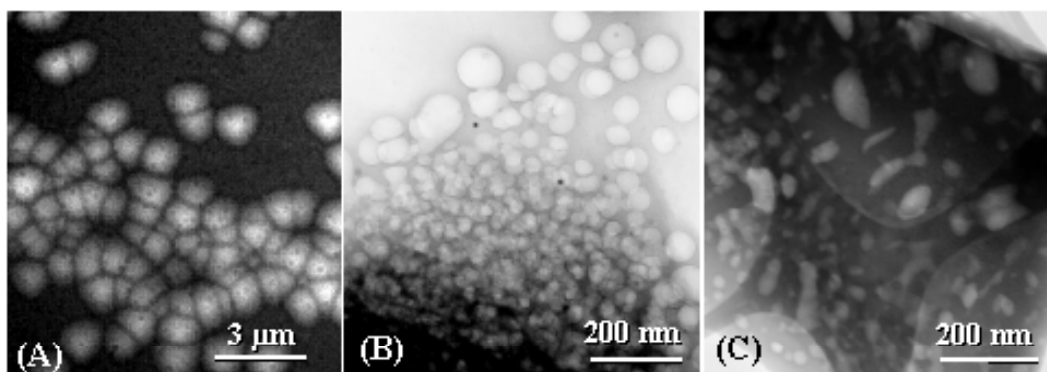


Fig. 5 TEM micrographs showing radiation-induced bubbles in sheet silicate and zeolites. (A) biotite (mica) after 800 keV  $\text{Kr}^{2+}$  irradiation to  $1 \times 10^{15}$  ions/cm<sup>2</sup> at room temperature; (B) analcime (zeolite) and (C) natrolite (zeolite) after 200 keV electron irradiation at room temperature.

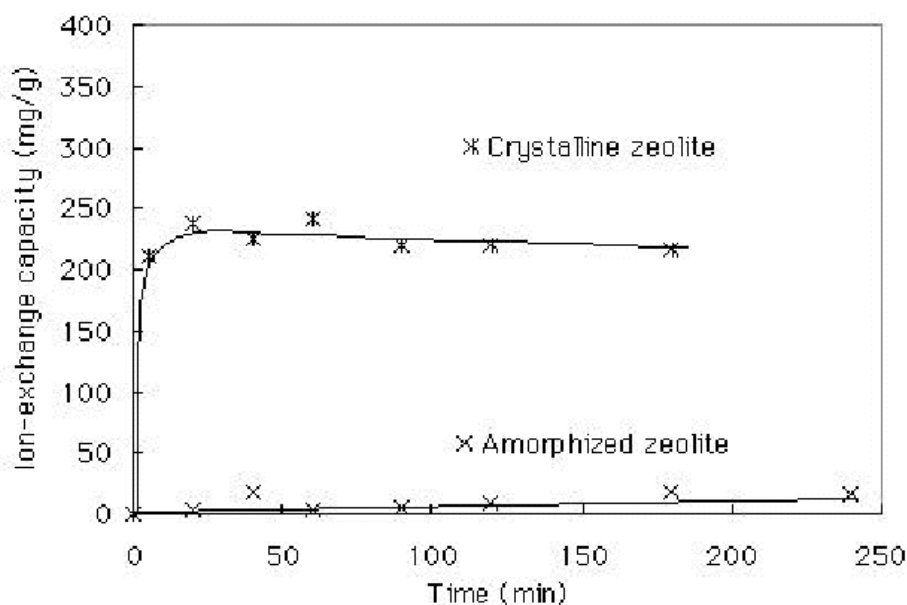


Fig. 6 Variation of ion exchange capacity for Cs in crystalline and amorphous zeolite-NaY.

However, thermally-induced and radiation-induced amorphous phases may have different structures and compositions, as well as physical and chemical properties (e.g., during the thermal process, the water vapor may be much more efficiently released from the structure than during the irradiation processes). As such, quantitative relationship between the radiation dose and the ion exchange capacity for radionuclides in concerned phases has not yet been established. More efficient irradiation sources and better designed experiments are needed to simulate the long-term radiation effects (on relatively larger volumes of sample) over relatively short periods.

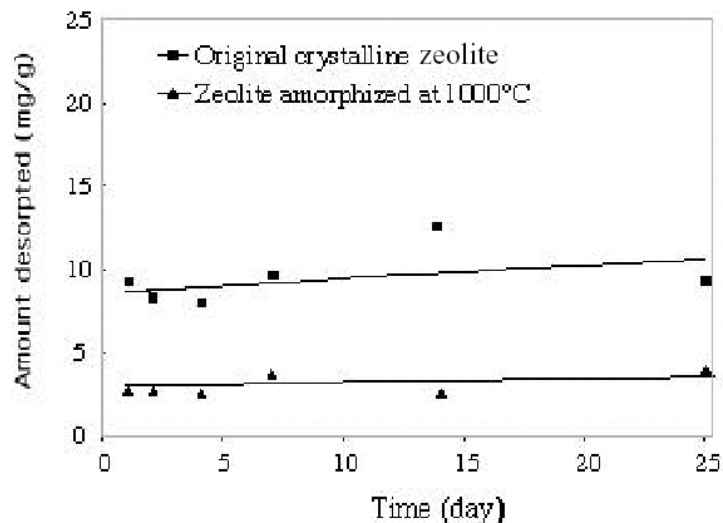


Fig. 7 Desorption of Cs ions from crystalline and thermally amorphized zeolite-NaY. Both samples were loaded with ~20 wt. % of Cs before the desorption experiment.

## Research Progress (2001-2003)

### 1. Neutron irradiation of zeolites

Twenty four zeolite samples have been irradiated to eight various doses in the Ford Nuclear Reactor (FNR) with thermal neutrons up to  $4.5 \times 10^{19}$  n/cm<sup>2</sup>. One third of the samples were preloaded with Sr and another one third was preloaded with Cs. These nuclides are important because: 1.) they represent a range of sorptive behavior that should bracket the behavior of most other radionuclides and 2.) they are considered to make important contributions to total radiation exposures, as illustrated in the Total Systems Performance Assessment-Viability Assessment of the proposed repository at Yucca Mountain. Ion exchange/sorption experiments are being conducted for samples irradiated to various doses to determine the impact of the radiation effects on the sorption capacity and retention of radionuclides. The irradiated material are also being characterized by a wide variety of analytical techniques (e.g., magic angle spinning nuclear magnetic resonance spectroscopy, x-ray diffraction, X-ray absorption spectroscopy, and X-ray absorption spectroscopy) to precisely describe the nature of the radiation damage at the near atomic-scale. These analysis combined with the sorption and cation-exchange results are providing important information for determining the relationships among key parameters: radiation damage dose, microstructure at the surface, materials properties (e.g., aperture size of the zeolites), and radionuclide sorption and/or ion exchange.

#### 1.1 MAS NMR analysis

In the research work, high-resolution solid-state MAS NMR (magic angle spinning nuclear magnetic resonance) spectroscopy was performed on original and strontium loaded zeolites since MAS NMR is a powerful tool in providing the coordination number change or distortion of the tetrahedron under neutron irradiation. Figure 8 and 9 show the

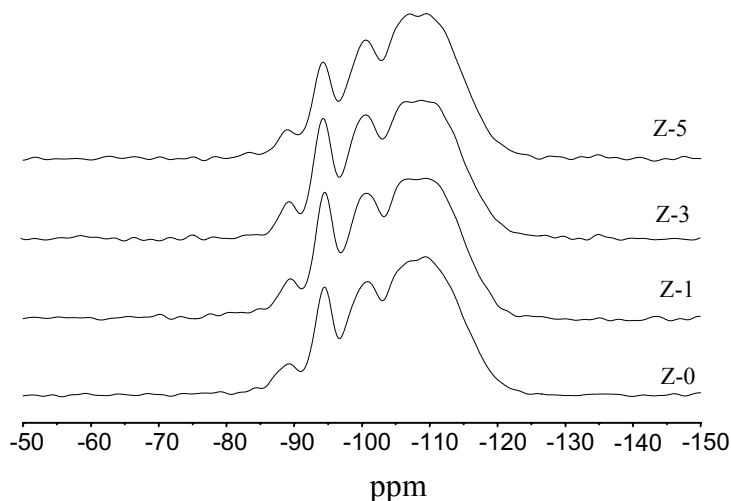


Fig. 8  $^{29}\text{Si}$  MAS NMR spectra of Z-series zeolite at different neutron irradiation dose levels (Z-0: unirradiated, Z-1:  $3.25 \times 10^{18} \text{ n/cm}^2$ , Z-3:  $1.25 \times 10^{19} \text{ n/cm}^2$ , Z-5:  $2.25 \times 10^{19} \text{ n/cm}^2$ ).

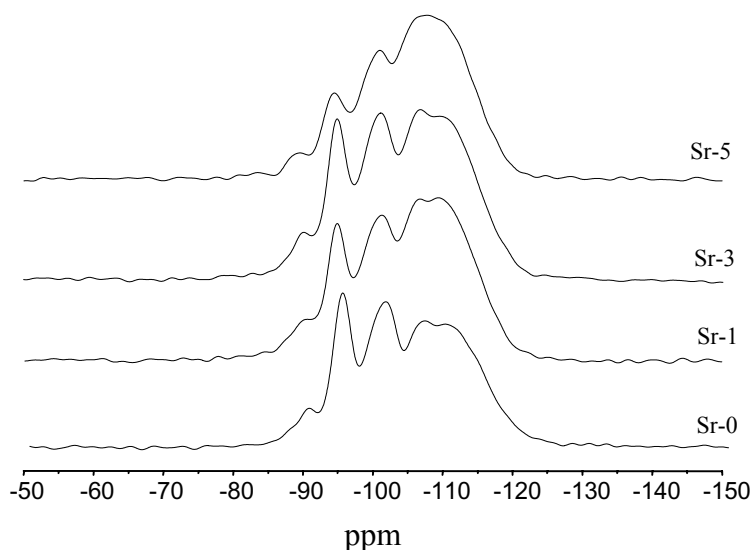


Fig. 9  $^{29}\text{Si}$  MAS NMR spectra of Sr-series zeolites at different neutron irradiation dose levels (Sr-0: unirradiated, Sr-1:  $3.25 \times 10^{18} \text{ n/cm}^2$ , Sr-3:  $1.25 \times 10^{19} \text{ n/cm}^2$ , Sr-5:  $2.25 \times 10^{19} \text{ n/cm}^2$ ).

MAS NMR spectra of the two series zeolites before and after neutron irradiation (at different dose levels). As we know, zeolite three-dimensional framework is consisted by  $[\text{SiO}_4]$  or  $[\text{AlO}_4]$  structural unit. The replacement of one or more Si by Al in the second coordination sphere would result in significant low-field shifts (i.e., less negative  $\delta$  values). In general, each substitution of Al-O-Si to Si-O-Si (Loewenstein rule forbids the two tetrahedrally coordinated aluminum atoms on neighboring T positions (Loewenstein, 1954), so there is no bond of Al-O-Al in synthesized zeolites) brings about a deshielding of ca 5 ppm for central silicon atom. Thus the different chemical shifts in the  $^{29}\text{Si}$  MAS NMR spectra are resulted from the contribution of different secondary coordination number of Al atoms. The deconvolution of one of the present  $^{29}\text{Si}$  MAS NMR spectra is shown in Figure 10. From the spectrum and other deconvoluted spectra

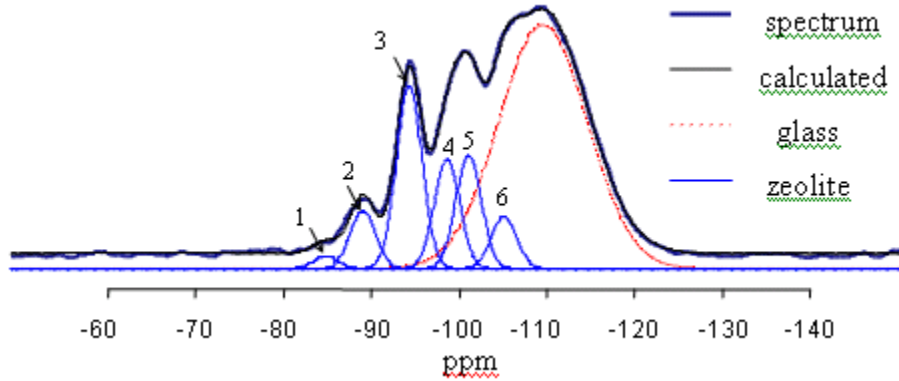


Fig. 10 Deconvolution of  $^{29}\text{Si}$  MAS NMR spectrum of Zeolite-NaY (1-Si(4Al), 2-Si(3Al), 3-Si(2Al), 4-Si(1Al), 5-Si(1Al), 6-Si(0Al)).

(not shown), it suggests that the second coordination number of Al in the present two series zeolites are 4, 3, 2 and 1, respectively. The intensities of the peaks can be used to calculate the overall Si/Al ratio of the framework according to the following formula:

$$\frac{Si}{Al} = \frac{\sum_{n=0}^4 I_n}{\sum_{n=0}^4 \frac{n}{4} I_n} \quad (1)$$

where  $I_n$  is the intensity of the peak associated with Si( $n$ Al). The Si/Al ratio of original zeolites (Z series) and strontium loaded zeolites (Sr series) with neutron irradiation dose are shown in Figure 11. Noting that the original Si/Al ratio of the zeolite provided by the purchased company (Zeolyst International) is 2.55, we found that the result 2.57 is rather accurate. Thus, we concluded that the neutron irradiation lead to the mild dealumination of the two zeolites. The chemical shift of the two series zeolites are tabulated in Table 1. We find the most apparent chemical shift value changes occurred in Si(4Al) for both series. The chemical shift values for other secondary aluminum polyhedra do not change so much comparing with those in Si(4Al). However, it can be seen that all the chemical shifts become less negative with the increase of neutron dose level. To our knowledge, the present MAS NMR research on neutron-irradiated zeolites is the first conducted work. Other MAS NMR work of neutron irradiation effect mainly focused on  $\text{SiO}_2$ . Chan *et al.* found that the chemical shift of  $^{29}\text{Si}$  MAS NMR changed from -107.1 ppm to -106.0 ppm when the neutron dose increased from  $1.99 \times 10^{17}$  to  $8.7 \times 10^{19}$  n/cm<sup>2</sup> in quartz (Chan *et al.* 1988). Wright *et al.* found that the chemical shift of  $^{29}\text{Si}$  MAS NMR became less negative when vitreous silica was subjected to a dose of  $2.8 \times 10^{20}$  fast neutrons/cm<sup>2</sup> (Wright *et al.*, 1992). By calculation, they found the average Si-O-Si bond angle decreased around 9.5°.

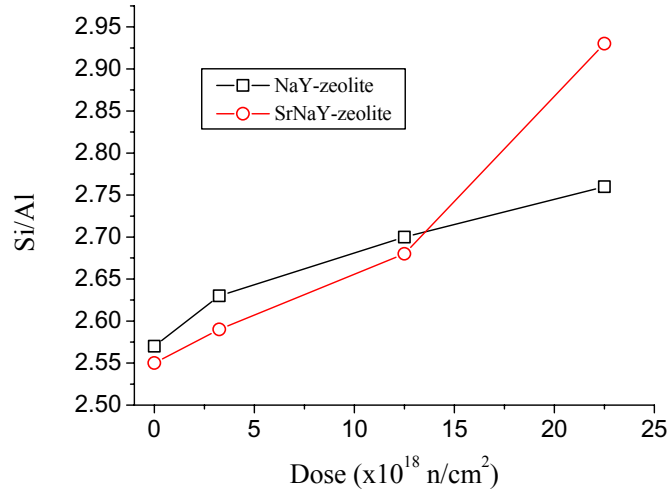


Fig. 11 Variation of Si/Al in Z series and Sr series with neutron irradiation dose.

**Table 1. Chemical shift in  $^{29}\text{Si}$  MAS NMR Spectra- $\delta$  (ppm)**

Samples	Si (4Al)	Si (3Al)	Si (2Al)	Si (1Al)	Si (1Al)	Si (0Al)
Z-0	-86.43	-89.38	-94.35	-98.59	-101.07	-105.07
Z-1	-84.50	-89.34	-94.50	-98.94	-101.40	-105.39
Z-3	-84.40	-89.36	-94.41	-98.81	-101.25	-105.33
Z-5	-83.83	-89.09	-94.17	-98.44	-100.84	-105.16
Sr-0	-87.08	-90.17	-94.68	-98.70	-101.17	-105.43
Sr-1	-86.65	-90.21	-94.75	-98.84	-101.40	-105.50
Sr-3	-86.71	-90.13	-94.79	-98.88	-101.39	-105.67
Sr-5	-83.07	-89.25	-94.35	-98.45	-100.96	-105.21

The correlations between chemical shift and mean Si-O-Si bond angle was first suggested by Thomas *et al.* (Thomas *et al.*, 1982). Smith and Blackwell first reported empirical correlations between the chemical shift shifts for aluminum silicate (Smith and Blackwell, 1983). Thomas *et al.* (Thomas *et al.*, 1983) and Engelhardt *et al.* (Engelhardt *et al.*, 1984) have found different semi-empirical chemical shifts–T-O-T correlation in different zeolites, respectively. However, the relationships are limited to silicon rich zeolites. Ramdas and Klinowski (Ramdas and Klinowski, 1984) were the first people reported a relationship which are valid for chemical shifts in all five Si(4Al), Si(3Al), Si(2Al), Si(1Al) and Si(0Al) tetrahedral environments, and also holds for the Si(0Al) shifts in silica polymorphs listed by Smith and Blackwell (Smith *et al.* 1983). Radeaglia and Engelhardt reported another relationship (Radeaglia and Zengelhardt., 1985). Both of their relationships are in agreement with experimental findings. Equation (2) is derived from Ramdas and Klinowski:

$$\delta = 126.6 + 5.6n - 247.5 \sin \theta \quad (2)$$

where  $\delta$  is the chemical shift,  $n=0, 1, 2, 3, 4$  in  $\text{Si}(n\text{Al})$  tetrahedral environment,  $\theta$  is the Si-O-T (T=Si, Al) bond angle. According to this equation, the Si-O-T angle of neutron irradiated zeolites and strontium-loaded zeolites are listed in Table 2. It displays that the bond angle of Si-O-Al in  $\text{Si}(4\text{Al})$  decrease from  $144.1^\circ$  to  $140.4^\circ$  for Z series while that of Sr series decrease from  $145.1^\circ$  to  $139.3^\circ$ . The changes of other Si (3Al) is not

**Table 2 T-O-T angles of zeolite-NaY/zeolite-SrNaY under different neutron dose**

Samples	Si (4Al)	Si (3Al)	Si (2Al)	Si (1Al)	Si (1Al)	Si (0Al)
Z-0	144.07	140.28	139.43	137.65	140.95	138.79
Z-1	141.94	140.23	139.63	138.10	141.41	139.22
Z-3	141.13	140.38	139.51	137.93	141.20	139.14
Z-5	140.35	139.89	139.19	137.45	140.64	138.91
Sr-0	145.05	141.37	139.87	137.79	141.09	139.27
Sr-1	144.40	141.42	139.97	137.97	141.41	139.36
Sr-3	144.49	141.35	140.02	138.02	141.40	139.59
Sr-5	139.32	140.10	139.43	137.47	140.80	138.98

obvious for Z-series (as shown in Figure 12), but for Sr-series, there is still  $1.27^\circ$  difference between Sr-0 and Sr-5. Although the changes for other Si ( $n\text{Al}$ ) ( $n=0, 1, 2$ ) are not so large compared with  $\text{Si}(4\text{Al})$ , generally, the Si-O-T bond angle decrease with increase of neutron exposure. Obviously, in the present dose range, Si-O-Al is more sensitive to neutron irradiation, Si-O-Si seems more rigid than Si-O-Al. This may be the reason the  $10^{20}$  order of dose level was applied in many researches on neutron irradiation of  $\text{SiO}_2$  in order to lessen the bond angle of Si-O-Si. The decrease of Si-O-Al bond angle will lead to the increase of Al-O bond length or increase of coordination number of aluminum polyhedron. The phenomenon decrease in Si-O-T bond angle is the same as the above mentioned neutron-irradiation in quartz and vitreous silica. Also, the decrease of Si-O-T bond angle is found in the high pressure induced amorphization in zeolites (Huang, 2001; Huang, 1998). This suggests that there are some similarities between irradiation- and high pressure-induced amorphization in zeolites in short or intermediate range.

Figure 13 and 14 are the  $^{27}\text{Al}$  NMR spectra of Z-series and Sr-series zeolites. It can be seen that when the dose level reached  $2.25 \times 10^{19} \text{ n/cm}^2$ , six-folded aluminum polyhedron emerged in both spectra (small peaks indicated by arrows in both Figure 13 and 14). This is consistent with the dealumination conclusion drawn from the Si/Al ratio obtained from the  $^{29}\text{Si}$  MAS NMR spectra above. The chemical shift values are listed in Table 3. A complication of  $^{27}\text{Al}$  MAS NMR spectrum is the second order quadrupolar interaction of the central transition. As a result, resonances move from their isotropic chemical shift due to the quadrupolar induced shift and broaden into specific powder line shapes, even under MAS conditions. Hence, the  $^{27}\text{Al}$  MAS NMR spectra may consist of resonances shifted with respect to their isotropic chemical shifts, which are not well-resolved, and even some aluminum may escape detection due to extreme broadening. Therefore, care must be taken when interpreting  $^{27}\text{Al}$  MAS NMR spectra. Lippmaa *et al.* found semi-empirical chemical shifts Al-O-Si correlation considering the correction of the second order quadrupolar interaction effect (Lippmaa and Magi, 1986):

$$\delta_{CS}(Al) = -0.50\theta + 132 \quad (3)$$

where  $\theta$  is the bond angle of Al-O-Si. According to this relationship, the corrected chemical shifts of aluminum are listed in last column in Table 3. Obviously, the chemical shifts changing trends for both series after second order quadrupolar interaction corrections are the same as those of silicon (*i.e.*, the bond angle of Al-O-Si decrease upon neutron irradiation).

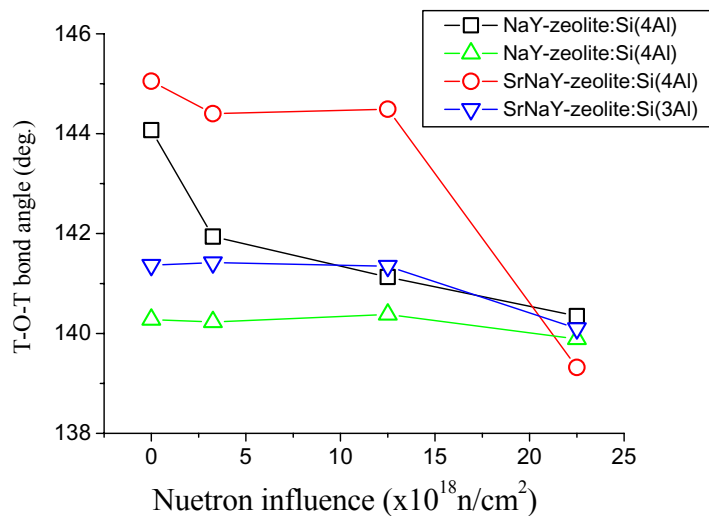


Fig. 12 Variation of T-O-T bond angles of different secondary coordinated polyhedral with neutron influence.

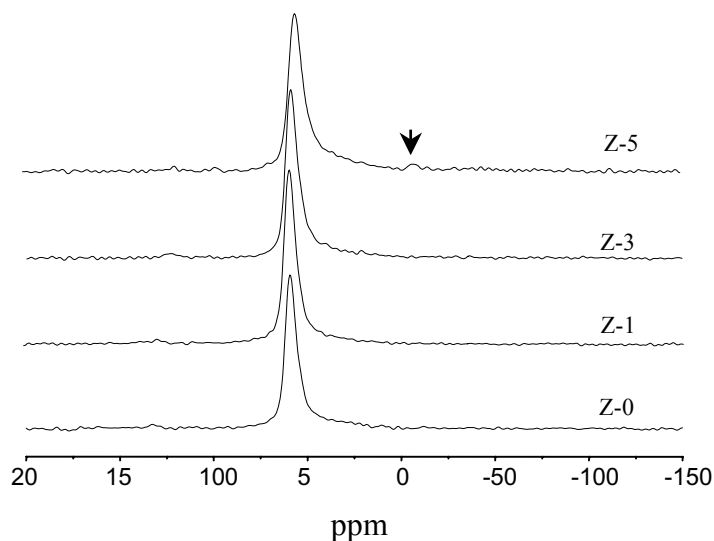


Fig. 13  $^{27}\text{Al}$  MAS NMR spectra of Z-series zeolites at different neutron irradiation dose levels.

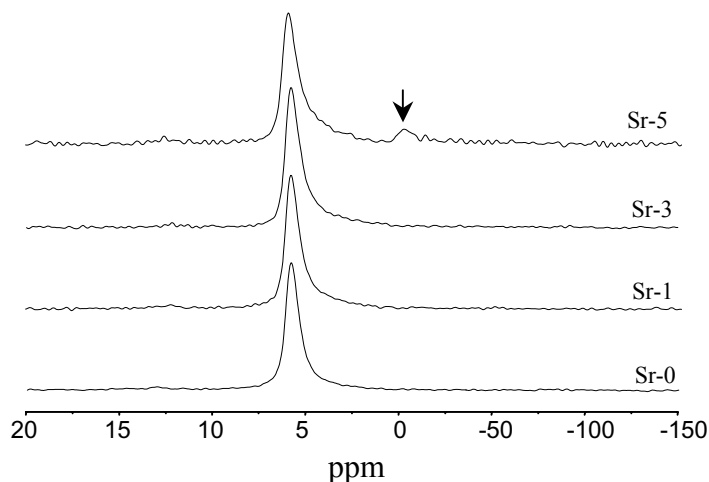


Fig. 14  $^{27}\text{Al}$  MAS NMR spectra of Sr-series zeolites at different neutron irradiation dose levels.

**Table 3 Chemical shift in  $^{27}\text{Al}$  MAS NMR Spectra- $\delta$  (ppm)**

Samples	$\text{Al}^{\text{tet}}$	$\text{Al}^{\text{oct}}$	Corrected $\text{Al}^{\text{tet}}$
Z-0	59.4	-	60.32
Z-1	58.9	-	62.09
Z-3	58.9	-	62.17
Z-5	55.2	-7.8	62.34
Sr-0	58.0	-	61.96
Sr-1	58.5	-	61.88
Sr-3	58.0	-	61.87
Sr-5	59.8	2.2	62.25

When comparing the  $^{27}\text{Al}$  MAS NMR spectra of Sr-series with that of strontium loaded zeolite treated at  $900^\circ\text{C}$  for 30 minutes (not shown), the  $^{27}\text{Al}$  NMR spectrum shows the peak maximum shifted upfield, ca -10 ppm, and the peak width (approximated FWHM) increased by more than 3 times. Both the substantial shift and increase in peak width and asymmetry are indicative of second order quadrupolar broadening. The additional shift of ca -10 ppm observed for the Sr-loaded, thermally treated sample indicates an increase in the quadrupolar coupling of approximately 2.8-3.2 MHz. This analysis of the change in the quadrupolar peak shape as well as the lack of any additional peak near 0 ppm suggests that the aluminum species in the thermally treated zeolite are in a highly distorted tetrahedral environment. Thus, the microstructure changes of the framework under neutron irradiation and thermal treatment are different.

It is believed that the origin of the octahedral aluminum is resulted from the  $\gamma$ -irradiation of the (n,  $\gamma$ ) process. Ali and Selim even found tricoordinated aluminum in  $\gamma$ -irradiated zeolites (Ali *et al.*, 1994; Selim *et al.*, 1992). Carvalho *et al.* attributed the dealumination of offretite under  $\gamma$ -irradiation to the presence of water in the sample since they did not observe the dealumination as the samples irradiated in vacuum. Instead, they found only crystallinity loss under vacuum condition. However, Durrani *et al.* indicated that the effect of  $\gamma$ -radiolysis is only significant at low doses up to 0.5 MGy, with little



change occurring as the dose was further increased (Durrani *et al.*, 1993). According to Primak *et al.*, when vitreous silica was irradiated by neutron irradiation, the estimated temperature (thermal spike) and pressure around the site of the primary knocked-on atom would be 5000~10000°C and 3000~7000 atm (Primak *et al.*, 1964). Thus, ballistic collision and ionizing are both possible reasons for the decrease of Al-O-Si bond angle and the formation of aluminum octahedron and thus result in the amorphization of the zeolites.

### 1.2 Ion exchange ability

The ion exchange capacity changes also indicate the neutron effect on the microstructure of zeolite. The equilibrium study for ion exchange capacity was carried out by placing zeolite-NaY samples in contact with SrCl<sub>2</sub> solution with initial concentration in the range of 0.2 mN to 2 mN. At equilibrium, the mass of solute adsorbed per unit mass of sorbent can be calculated from:

$$Q_e = \frac{(C_0 - C_e) \times L}{M_z} \quad (4)$$

where  $C_0$  is the original solution concentration,  $C_e$  is the equilibrium solution concentration,  $L$  is the volume of the solution in contact with zeolite-NaY,  $M_z$  is the mass of zeolite-NaY used in each experiment. Figure 15 is the ion exchange isotherms of SrCl<sub>2</sub> with original (untreated), neutron-irradiated (Z-5) and thermally treated (900°C, 30 minutes, x-ray amorphization) zeolite-NaY. It can be seen that the amorphous zeolite-NaY has lost almost all of the exchangeable sites while the original zeolite keep strong ion exchange ability with strontium ions. The ion exchange ability of Z-5 is between them. This indicates that some exchange sites in neutron-irradiated zeolite have already lost due to the possible breakage of the framework or contraction (collapse) of the cages in zeolite, but the changes is not so large as that of the thermally treated zeolite-NaY. This is consistent with the indication of MAS NMR results demonstrated above.

### 1.3 XAS (X-ray absorption spectroscopy) study

The local coordination environment of Sr sorbed on zeolite (NaY) before and after neutron irradiation was characterized using XAS (X-ray absorption spectroscopy). Neutron-irradiation was performed either before or after the Sr-loading to study the impact of the treatment on the sorption property of the mineral as well as the local structural changes around Sr.

In the experiment, zeolite powders were exposed to 0.2M SrCl<sub>2</sub> aqueous solution for 24 hours at room temperature. The Sr exchanged zeolites were rinsed with deionized water several times until no Cl<sup>-</sup> would be detected by AgNO<sub>3</sub> test. The Sr-zeolite was dried at 50°C for 120 and then was either neutron-irradiated (Sr-5, detailed procedure described elsewhere in this report) or heated at 900°C for 45 minutes (Sr-2-900) for the purpose of Sr environment comparison. N-5 was prepared by exposing the neutron-irradiated zeolite to 4mM SrCl<sub>2</sub> solution. The more dilute concentration was used as the pre-irradiated zeolite had lower exchange capacity.

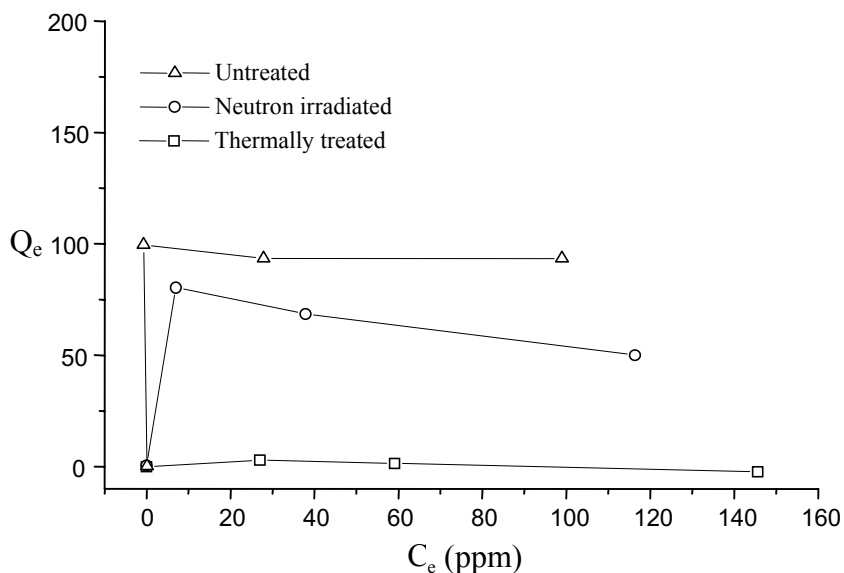


Fig. 15 The ion exchange isotherms for  $\text{SrCl}_2$  with original (untreated), neutron-irradiated (Z-5) and thermally treated ( $900^\circ\text{C}$ , 30 minutes, x-ray amorph) zeolite-NaY.

The Sr-preloaded and neutron-irradiated zeolite sample (Sr-5) has a very distinct and unique EXAFS and corresponding radial structure function (RSF) compared to aqueous  $\text{Sr}^{2+}$  ( $\text{SrCl}_2$ ) spectrum or that of Sr sorbed (N-5) on heated zeolites (Table 4 and Figure 16). For Sr-5, the EXAFS shows a distinct “beat” (shoulders on the main oscillations) with the Sr EXAFS fitting indicating the presence of first shell coordination of oxygen atoms and a second shell of Si/Al neighbors (Table 4). X-ray absorption near edge structure (XANES) analysis of Sr-5 also indicates that the neutron-irradiation affects the local environment of Sr compared to heat treated samples (Figure 17). A first derivative plot of the XANES shows different locations for peak features, strong evidence of different first shell coordination environment among the neutron-irradiated and heated treated zeolites at different temperatures. This noticeable difference in the XANES is consistent with the EXAFS data which together indicate that neutron-irradiation of previously loaded Sr (Sr-5) leads to a different Sr coordination environment compared to heat treatment (Sr-2-900) and Sr sorbed to the neutron irradiated sample (N-5). Interestingly, Sr sorbed to a previously neutron damaged sample (N-5), has a coordination environment similar to heat treated sample with similar CN and R for nearest neighbor oxygens and second nearest neighbor Al/Si. This suggests that on neutron damaged material Sr has limited access to the sites found for Sr-5. The comparison of Sr-5 with N-5 and Sr-2-900 also indicates that the neutron irradiation may have been long enough to affect some amorphization of the surface but not throughout the sample with this amorphization resulting in similar coordination of Sr in N-5 and Sr-2-900. Further investigations on samples that have had longer exposure to neutron irradiation are needed to determine if complete amorphization results from increased exposure to neutron irradiation.

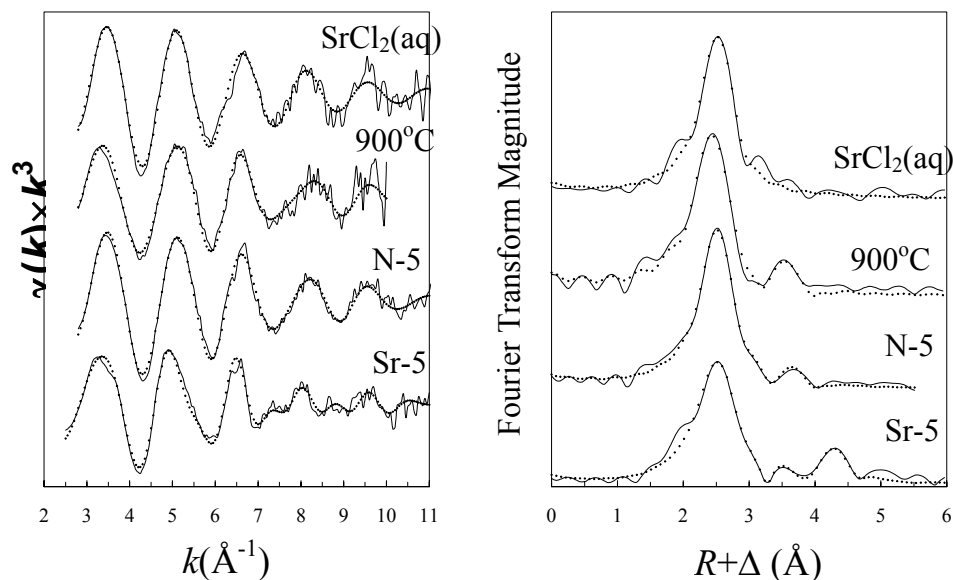


Fig. 16 Normalized EXAFS spectra and RSFs of strontium loaded zeolite. Sr-5: Neutron-irradiated Sr loaded zeolite ; N-5: 4mM Sr sobbed on neutron-irradiated zeolite;  $900^\circ\text{C}$ :  $900^\circ\text{C}$  heat treated Sr loaded zeolite.

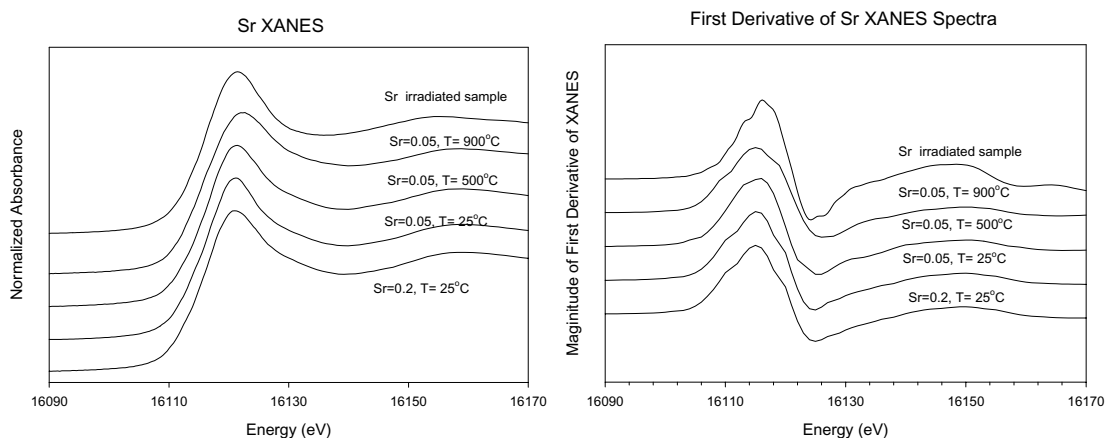


Fig. 17 Normalized XANES spectra and their first-derivatives for Sr-zeolites.

To more definitively interpret the local coordination environment of Sr in the neutron irradiated samples in lieu of the EXAFS results requires an assessment of how radiation damage is expected to impact the location of atoms in the Sr exchanged zeolite samples. Neutron particles are more likely to cause changes in the Sr and Al positions in the zeolite compared to other elements in the structure. Sr is fully hydrated and only weakly exchanged in the zeolite structure and should be the most vulnerable to the neutron bombardment. A scenario consistent with this notion is that Sr ions may move from the original  $\text{S}_{\text{IV}}$  site in the supercage to the other nearby positions in the framework of the zeolite. Since analysis in the EXAFS indicate a Sr local coordination environment that includes Si/Al neighbors after neutron irradiation (Table 4 and Figure 16), it is feasible that irradiation resulted in the movement of Sr due to the neutron bombardment. It is also

**Table 4. EXAFS fit results for Sr sorbed on zeolite before and after neutron-irradiation**

Sample	Sr-Z <sup>a</sup>	CN <sup>b</sup>	R <sup>c</sup>	$\sigma^2$ <sup>d</sup>	$\Delta E_0$ <sup>e</sup>	
<b>SrCl<sub>2</sub>(aq)</b>	Sr-O	8.699	2.58	0.01331	-5.927	0.01M SrCl <sub>2</sub> solution
<b>Sr-5</b>	Sr-O	9.551	2.60	0.01877	-8.303	Sr-zeolite neutron-irradiated
	Sr-Si/Al	5.470	4.34	0.01399		
	Sr-Si/Al	2.854	4.74	0.01399		
	Sr-Si/Al	1.771	3.42	0.01399		
	Sr-Si/Al	1.587	3.71	0.01399		
<b>N-5</b>	Sr-O	8.911	2.57	0.01331	-6.409	Neutron-irradiated 4mM Sr
	Sr-Si/Al	1.364	3.44	0.16000		
	Sr-Si/Al	1.947	3.79	0.16000		
<b>Sr_2_900</b>	Sr-O	7.581	2.54	0.01331	-10.384	Sr-zeolite 0.2M Sr 900°C
	Sr-Si/Al	1.466	3.37	0.01239		
	Sr-Si/Al	1.566	3.78	0.01239		

<sup>a</sup> Z = backscatterer; <sup>b</sup> CN = coordination number; <sup>c</sup> R = interatomic distance; <sup>d</sup>  $\sigma^2$  = Debye-Waller factor; <sup>e</sup>  $E_0$  = Energy at  $k = 0$

likely that the neutron bombardment selectively moves tetrahedral Al(III) from the framework of [Al, Si]O<sub>4</sub> tetrahedra compared to tetrahedral Si(IV) due to the larger size and lower stability of Al compared to Si in the tetrahedra. Consistent with these expectations, we interpret the local coordination environment for Sr to include associations of Sr with the oxygens from octahedral Al clusters formed by Al that has been moved from its tetrahedral positions to the supercage of the zeolite structure following neutron bombardment. Octahedral coordination of Al in Sr-5 has been confirmed by <sup>27</sup>Al MAS NMR study stated previously. An NMR peak at a chemical shift near 0 ppm in that study has been assigned to octahedrally coordinated Al(III), which is consistent with Sr association with aluminum clusters in octahedral coordination in the supercage. Taken together, these data are consistent with Sr in neutron-irradiated Sr-zeolite bound to the S<sub>II</sub> site located above the center of the hexagonal face of sodalite unit, with Sr coordinated to six oxygen(s) of the hexagon of oxygens that include oxygens left behind from the Al leached from the tetrahedral positions and three oxygens from Al-octahedra subsequently formed in the supercage.

Despite the difference in the local coordination of Sr in the neutron irradiated samples, synchrotron XRD data of sample Sr-5 (Figure 18) indicate that the neutron irradiated zeolite sample retains some of its original structure (signature peaks for the zeolite are still present in spectrum as well as additional peaks in the XRD, some of which are consistent with Al-octahedral phases). Although Sr has CN and R values for nearest neighbor oxygen atoms similar to those of aqueous Sr or Sr sorbed on untreated zeolite (Table 4), the neutron irradiated Sr samples also have Si/Al neighbors at 3.44Å and 3.79Å (compare Sr-5 to SrCl<sub>2</sub>). This close association of Sr with Si/Al in the irradiated samples indicates that even though some of the supercage structure is retained that Sr has formed a stronger association that is less accessible for ion exchange compared to undamaged samples. These results indicate that irradiation causes previously

exchangeable Sr to become less exchangeable after damage, regardless of the radiation source, a desirable result from a waste management perspective.

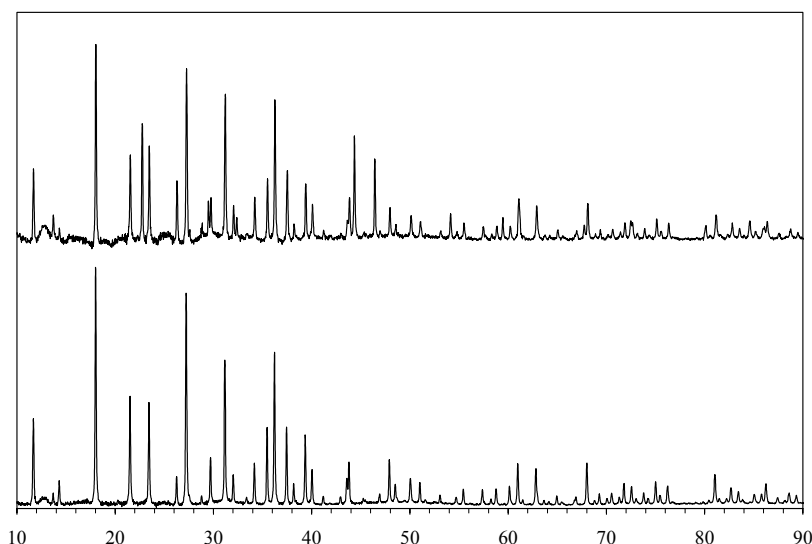


Fig. 18 Synchrotron XRD pattern of neutron-irradiated (up) and unirradiated (down) strontium loaded zeolites.

In summary, Si-O-T bond angle decrease with the increase of neutron-irradiation dose level. At the same dose level, the Si-O-T bond angles change in zeolite-SrNaY are larger than those of zeolite-NaY. This may due to the effect of strontium on the framework bond property in zeolites. From the bond angle changing trend, it is expected that at higher dose levels, Si-O-Si bond angle will decrease. Under neutron irradiation, mild dealumination occurs. It is also found that  $[AlO_6]$  formed at higher dose level. The ion exchange results show that the ion-exchange ability of neutron irradiation zeolite is between the original (untreated) and amorphous (thermally treated) zeolite. This suggests that the ion-exchange sites begin to lose due to the microstructure changes in the framework under neutron irradiation. The XAS study on neutron-irradiated zeolite samples show that neutron-irradiation has a different impact on the structure and sorption property of zeolite compared to heat treatment. Synchrotron XRD shows that the neutron damaged zeolite maintains some of its original structure but additional features on the XRD compared to untreated samples that indicate some of the zeolite has been converted to other phases including the possibility of octahedral Al phases. Given that the coordination environment of Sr sorbed on neutron damaged zeolite was similar to the heat treated Sr sample (known to be completely amorphized), suggests that partial amorphization may have occurred in neutron irradiation samples.

## 2. Proton irradiation of zeolites

### 2.1 DRIFT and XPS works

In this section, zeolite-NaY powders were pressed to form tablets which were 2 cm in diameter and 1.5 mm in thickness. The zeolite tablets were irradiated with a 500 keV  $H^+$  beam at the dose rate of  $5 \times 10^{12}$  ions/s for 10, 20 and 30 hours, respectively. The cumulative doses were measured with a Faraday cap, which yielded total doses of  $2 \times 10^{17}$ ,  $4 \times 10^{17}$ , and  $6 \times 10^{17}$  ions/cm<sup>2</sup> for the three samples, respectively. The microstructural

changes of zeolite-NaY before and after proton irradiation was characterized by using diffuse reflectance Infrared Fourier transformation (DRIFT). Also, the x-ray photoelectron spectroscopy (XPS) works on the evolution of the microstructure as a function of displacive radiation dose have been conducted.

Figure 19 is the DRIFT spectra of proton-irradiated zeolite-NaY at different dose levels. It can be seen that there are three apparent bands at 468, 1040 and 1153  $\text{cm}^{-1}$  in unirradiated sample. According to the classification of Flanigen (Flanigen, 1971), these three bands assign to T-O bending mode, asymmetric stretching mode (internal tetrahedra) and asymmetric stretching mode (external tetrahedra), respectively. Among them, the 468  $\text{cm}^{-1}$  T-O bending vibration and 1040  $\text{cm}^{-1}$  T-O asymmetric stretching vibration are structural insensitive, whereas 1153  $\text{cm}^{-1}$  T-O asymmetric stretching vibration is structural sensitive. Thus it is not surprised that when zeolite-NaY was subjected to proton irradiation, this structural sensitive band turned into a broadening shoulder with increase of irradiation dose level. This suggests that the connection between  $\text{TO}_4$  tetrahedra become less order.

The striking observation regarding the structural evolution is that the structural insensitive bands at 468 and 1040  $\text{cm}^{-1}$  rapidly lose intensity and broaden with the increase of irradiation dose. After irradiated for 30 hours, the band belonging to T-O bending vibration even disappeared. Since the bend mode appearing at 468  $\text{cm}^{-1}$  and the stretching mode at 1040  $\text{cm}^{-1}$  belong to the structural insensitive, the changes of structural insensitive bands show the changes of basic structural units of the framework in the zeolites. This is quite different from those of thermal-treated, high pressure and high-energy ball milling induced amorphization of zeolites, in which only the structural sensitive bands changed (Flanigen, 1971; Huang, 1998; Auroux *et al.*, 1996). Therefore, besides altering the connectivity of the tetrahedra, the broadening and loss of DRIFT intensity suggest a breakdown in the  $\text{TO}_4$  building units of the zeolitic framework and turns it into a disordering (amorphous) state. This indicates that the amorphization induced by proton irradiation is actually “more disorder” than the thermally treated samples. It is interesting that after zeolite-NaY was irradiated for 30 hours, a broadening band reappeared at 1133  $\text{cm}^{-1}$ . This may be due to the rebonding of the broken T-O at higher density of broken T-O linkages.

Although it is difficult to distinguish  $\text{AlO}_4$  from  $\text{SiO}_4$  in  $\text{TiO}_4$  intratetrahedral modes from the spectrum (Stubican. and Roy, 1961; Szostak and Thomas, 1986), through the shift of bands in infrared spectrum, we can know the changes of Al/Si in the framework. Indeed, there are some reports on a nearly linear decrease for the position of the main asymmetric stretching vibration with increasing atomic fraction of aluminum in the tetrahedral sites in faujasite-type framework (Flanigen, 1971). Since the mass of aluminum and silicon are nearly the same, the decrease in frequency (wave number) with increasing aluminum concentration appears to be related to variation in bond length and bond order. The longer bond length of Al-O and less electronegativity of aluminum result in a decrease in force constant. In the IR study of thermally treated zeolite-NaY, Flanigen *et al.* found that the asymmetric stretching band increased from 1000  $\text{cm}^{-1}$  at 85% x-ray crystallinity to 1020  $\text{cm}^{-1}$  at x-ray amorphization (Flanigen, 1971).

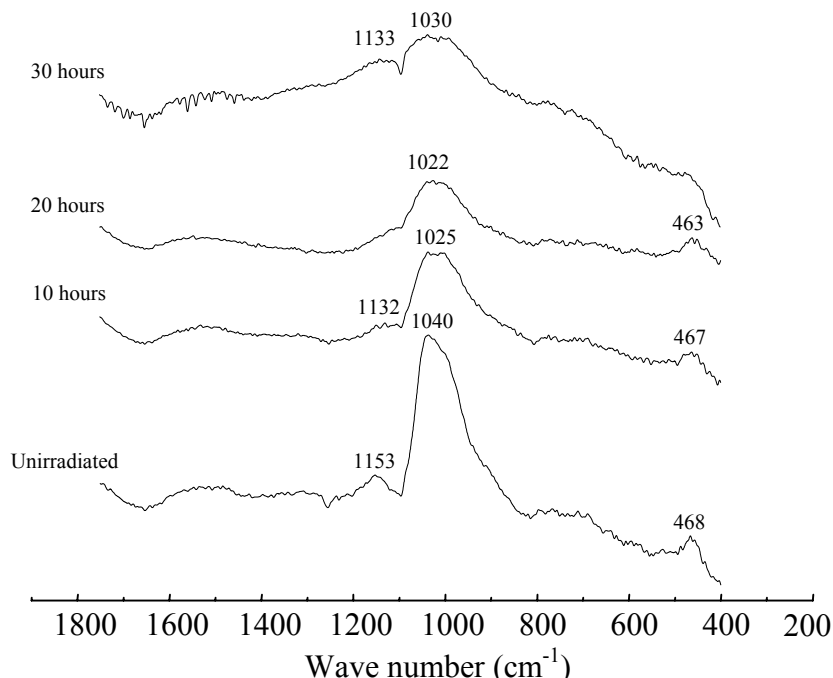


Fig. 19 The DRIFT spectra of proton-irradiated zeolite-NaY.

Thermal treatment process for hydrated zeolite is a dealuminum process for zeolitic framework. Thus, the decrease in Al/Si would lead to the increase for the position of the main asymmetric stretching vibration. However, from Figure 9, we see that after proton irradiation for only 10 hours, the asymmetric stretching vibration shifts from  $1040\text{ cm}^{-1}$  to  $1022\text{ cm}^{-1}$ . This changing trend suggests the increase of aluminum content in the zeolitic framework, which suggests that more Si-O bonds were broken compared with Al-O bonds when the irradiation time increased. This is reversible to that occurs in thermal treatment process. Up till now, most of the mechanisms proposed for ionizing radiation-induced damage are associated with the breakage of Al-O bonds in the zeolitic framework under electron irradiation (Bursill *et al.*, 1980, Treacy and Newsam, 1987). To the best of our knowledge, our DRIFT result is the first experiment evidence of the breakage of Si-O bonds in zeolitic framework under proton irradiation. In fact, in the bond-type criterion for the bombardment-induced structural changes in non-metallic solids, Naguib and Kelly have already pointed out that Si-O bonds are easier to be broken than Al-O bonds (Naguib and Kelly, 1975). In the study of fast neutron-metamict quartz, Qin *et al.* found a possibility of reduction in the average coordination number of silicon from the radial distribution functions obtained from energy-filtered electron diffraction data (Qin and Hobbs, 1995).

Recently, Cambor *et al.* found that the isomorphous substitution of Si by Al in the zeolitic framework resulted in the contraction of the framework (Cambor *et al.* 1996; Hong *et al.*, 1997). Since the bond length of Al-O ( $0.17\text{-}0.178\text{ nm}$ ) is longer than that of Si-O ( $0.157\text{-}0.167\text{ nm}$ ), they contributed the contraction of the framework to the decrease of bond angle of Si-O-T. From other related researches (Hosono, 1991; Devine and Marchand, 1993), it was found that the band shifts to lower frequency in IR spectra. This suggests the decrease in Si-O-T bridging bond angle. We could approximately calculate

the changes of the bridging bond angle according to a central-force idealized continuous-random-network theory (Sen, 1977; Galeener, 1979):

$$f^2 = (K / m_o)(1 - \cos \theta) + (4K / 3m_T) \quad (5)$$

where  $f$  is the angular frequency,  $m_o$  and  $m_T$  are the masses of the oxygen and network former atoms, respectively.  $K$  is the T-O bond stretching force constant. For small changes in  $\theta$ ,  $\Delta \theta$  can be related to  $\Delta f$  by differentiation Equation (5):

$$\Delta f = (k / m_o) \times \sin \theta \times (\Delta \theta / 2f) \quad (6)$$

Putting  $K=665$  N/m and  $\bar{\theta}=142^\circ$  for zeolite-NaY, according to the equation, the changes of Si-O-T bond angle after being subjected to proton irradiation are listed in Table 5. It can be seen that proton irradiation result in the decrease of Si-O-T bond angles. This is consistence with the observation of the above neutron irradiation in zeolites.

**Table 5 Change in Si-O-T with different irradiation dose**

Sample	$\Delta f_1^*$ (cm <sup>-1</sup> )	$\Delta \theta$ (deg)	$\Delta f_2^{**}$ (cm <sup>-1</sup> )	$\Delta \theta$ (deg)
1	15	-3.9	21	-6.1
2	18	-4.8	-	-
3	10	-2.7	20	-6.1

\* reference to the peak position at 1040 cm<sup>-1</sup>

\*\* reference to the shoulder position at 1153 cm<sup>-1</sup>

The XPS results of proton irradiated zeolite-NaY support the findings in the above DRIFT spectra.

As shown in Figure 20. After proton irradiation, a peak emerges at the lower binding energy side of the Si 2p XPS spectra. The decrease in binding energy of an element is the consequence of the increase in the effective negative charge on it (Chen *et al.*, 2001). In the present case, the decrease in binding energy of Si 2p electrons indicates an increase in the average electron density on the silicon ions, which implies that the shortening of the Si-O bond length. This can be achieved by the distortion or the decrease of coordination number of silicon tetrahedra. Figure 20 also displays the Si 2p electron XPS spectrum of thermally treated zeolite-NaY (X-ray amorphization). Unlike those of proton-irradiated samples, the Si 2p electron XPS spectrum is characterized by only one peak and its binding energy value is nearly the same to that of untreated zeolite-NaY. This strongly suggests that the silicon tetrahedra be kept after thermal treatment. It should be noted that after irradiated by proton for 30 hours, the intensity of the XPS peak located at lower binding energy side is reduced. This consists with the results of DRIFT spectrum of the same sample. As already stated above, the stochastic rebonding of the damaged structure will occur when there is an enough density of broken Si-O linkages. However, the less intense and more broaden peak in the spectrum suggest the disordering exists in the small range. This means proton induced amorphization is more disorder than that of thermal treatment induced amorphization.



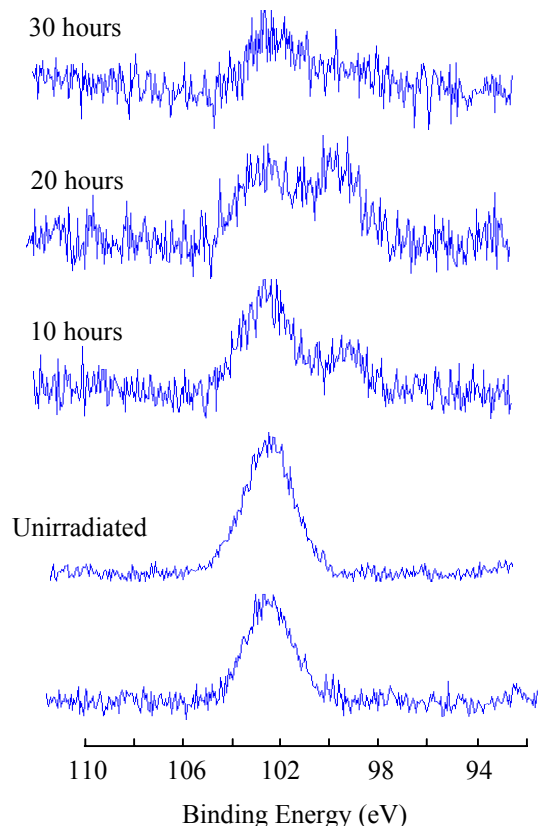


Fig. 20 The Si 2p XPS spectra of proton irradiated or thermally treated zeolite-NaY.

The similar results can be obtained from the Al 2p electron XPS spectra of proton-irradiated samples (not shown). Like Si 2p XPS spectrum, the emergence of the peak at lower binding energy side of Al 2p spectrum indicates the distortion or the changes of the coordination number of aluminum polyhedra. After irradiated for 20 hours, the peak at lower binding energy even grows higher. This suggests more Al-O bonds breakages occurred at this stage. Further increase of irradiation time results in a closer distance of the two peaks. This suggests the rebonding of broken Al-O linkage.

## 2.2 Ion exchange capacity

To quantify the radiation effects on the ion exchange capacity of zeolite-NaY, we performed detailed measurement of the concentrations of Cs and other elements along the cross-section of the irradiated samples. The irradiated zeolite samples were placed in a 10 mM CsCl solution at room temperature for 25 hours without agitation. The solid:solution ratio was 50 mg zeolite:50 mL solution. Because the density of the pressed sample was only ~50% of the theoretical density, the samples contained a large amount of void space. The large inter-particle pore size allowed the CsCl solution to quickly diffuse into the interior of the samples and ensured that all the particles were in effective contact with the solution throughout the ion exchange experiment. Based on a previous study, a complete Cs-zeolite-NaY ion exchange reaction occurred almost instantly under stirred conditions. Figure 21 shows the variation of Cs-concentration as a function of depth from

the irradiated sample surface. For the sample irradiated for 20 hours, the Cs-concentration decreased gradually with increasing target depth and reached the lowest concentration (~1 wt.%) at 12  $\mu\text{m}$ , indicating that the ion exchange capacity decreased with increasing radiation damage. When the zeolite was irradiated for 30 hours, the region with the lowest Cs-concentration widened. However, the Cs-concentration did not decrease further with an increase of ionizing energy deposition; this suggests that once complete amorphization is reached, further radiation does not have an effect on the ion exchange capacity.

The concentration profiles in Figure 21 and the energy deposition profiles suggest that the radiation damage to the zeolite by energetic protons is dominated by an ionization mechanism in the low displacement rate region. According to Monte Carlo simulation with the SRIM 2000 code, the damage produced by nuclear collision processes should be restricted to a narrow band with an abrupt structural and Cs-concentration change in the region at the end of the ion range. However, the wide range of low Cs-concentration in the sample irradiated for 30 hours and the gradual decrease in Cs-concentration with increasing target depth in the 20 hour irradiated sample indicates that the extent of structural damage and the change in ion exchange capacity are a function of the ionizing radiation dose. For the sample irradiated for 10 hours, even at the peak damage region, the Cs-concentration did not reach a Cs-concentration as low as in the cases of higher dose irradiations.

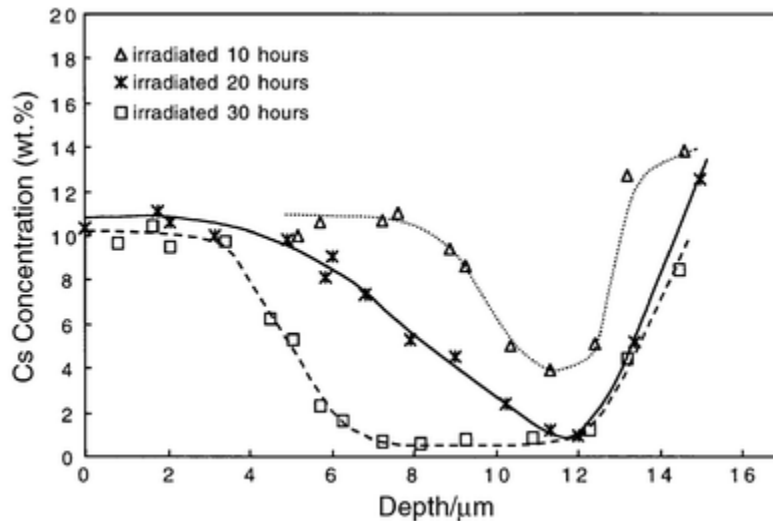


Fig. 21 The variation of Cs-concentration, as a function of target depth for the samples irradiated with 500 keV  $\text{H}^+$  for 10, 20 and 30 hours.

This result supports the suggestion that ionizing radiation is the dominant process leading to structural damage. The average Cs-concentration measured in the undamaged region was ~20 wt.%. A measurement of Cs-concentration in the point mode by EMPA showed that the average Cs-concentration in the bright spots is 30-50% higher than in the undamaged zeolite matrix. Figure 22 shows the change of concentration for all cations in the zeolite-NaCsY sample irradiated for 30 hours. Although the measured Na-concentration is lower than the actual concentration due to the migration of Na under the electron beam during the electron microprobe analysis, Figure 22 shows that the Na-

concentration profile moves in the opposite direction as compared with the Cs-concentration. No significant concentration changes were observed for Al and Si.

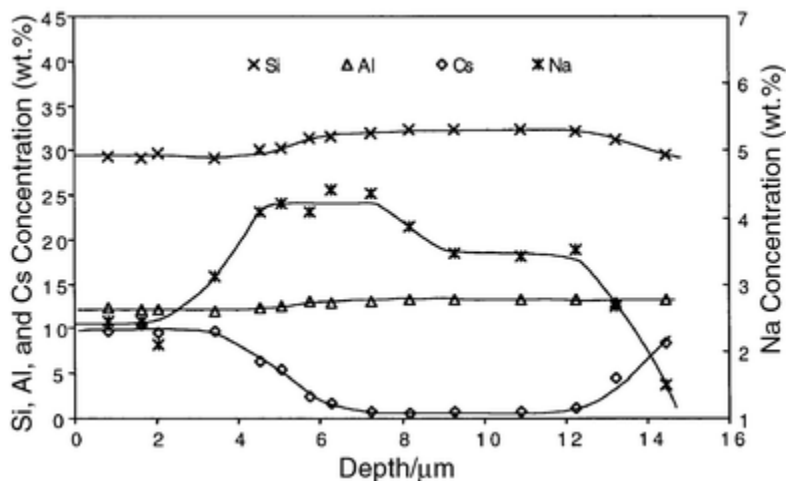


Fig. 22 Concentration profiles of major elements in the irradiated zeolite-NaCsY. The sample was irradiated with a 500 keV proton beam for 30 hours.

### 3. Thermal effects on zeolites

#### 3.1 XPS study

In the previous study, we found that the amorphized zeolite-NaY lost nearly 95% of its ion exchange capacity for Sr due to the loss of exchangeable cation species and/or the blockage of access to exchangeable cation sites. Also, the desorption study indicated that amorphization of Sr-loaded zeolite may enhance the retention capacity of exchanged Sr due to the closure of the channels. However, the microstructure considering the bonding environment is still missing. In this section, we have conducted the XPS work on the thermally treated zeolite-NaY and strontium-loaded zeolite (zeolite-SrNaY) in order to get more information about the structure changes of the zeolites under thermal treatment. We found that the binding energy value of  $\text{Sr}3d_{3/2}$  increases from 134.2 eV to 134.6 eV (Figure 23). From the available literature it can be conclude that the Sr-O distance varies between 0.2405 nm for the strongest bond and 0.2973 nm for the weakest bond. In a six-fold coordination (Sr(I)), the bonds are longer than in a threefold coordination of Sr(I') and Sr(II), which are similar. The difference in binding energy of  $\text{Sr}3d_{3/2}$  is the consequence of the difference of the effective negative charge on strontium. The lower the binding energy value, the higher the average electron density on strontium. The increase in binding energy of  $\text{Sr}3d_{3/2}$  indicates that the lower average electron density on strontium ion. This suggests strontium ions have diffused to sites I after SrNaY-zeolite has been treated at 900°C for 30 min. The rapid change of strontium coordination number brings the possibility in the breakage of some T-O-T bonds. The migration of strontium ions to sites I at higher temperature is benefit for the “capture” of strontium ions because the cations at sites I are stabilized by a large (0.5 Å) inward relaxation of the surrounding oxygen atoms (Georger *et al.*, 1991). For the amorphized zeolites-SrNaY, the collapse of the aperture would further prevent strontium ions from migrating out of the hexagonal

prisms. Both of the above reasons would be benefit for the immobilization of radionuclide  $^{90}\text{Sr}$ . At room temperature and 500°C, the spectra of Al2p can be fitted by

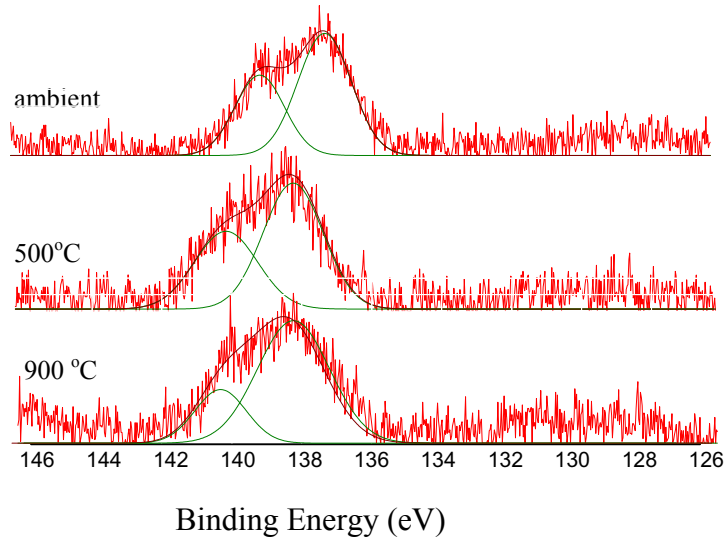


Fig. 23 The XPS Spectra of Sr 3d Photoelectron of Zeolite-SrNaY treated under Different Temperature (Mg  $K_{\alpha}$  x-ray source, electrical charging effect did not subtract in binding energy values).

one Gaussian function. This reveals that a symmetrical  $[\text{AlO}_4]^-$  polyhedra are still kept in the temperature range. However, when treating temperature is up to 900°C, a peak at lower binding energy side emerges. This suggests distortion of aluminum tetrahedron or aluminum polyhedron with other coordination number has occurred in the structure. The corresponding Auger parameter values of aluminum in zeolite-NaY, zeolite-SrNaY and zeolite-SrNaY (900°C) are listed in Table 6. In the study of aluminum coordination of dealuminated mordenites by x-ray photoelectron spectroscopy, Remy *et al.* deconvoluted the Al KLL auger spectra into three components (Remy *et al.*, 1993). The corresponding Auger parameters  $\alpha'$ , by adding these kinetic values of deconvoluted Al KLL peak with the binding energy of Al 2p, were in three different kinds of range: 1458.7~1459.3eV, 1459.8~1460.2eV and 1460.9~1461.5eV, respectively. They ascribed these three ranges to three kinds of III, IV and VI fold coordination of aluminum in zeolite. Collignon *et al.* probed the coordinated state of aluminum in  $\beta$ -zeolite by using similar method. Compared with the results of Remy and Collignon *et al.* (Collignon *et al.*, 2001), we found that our Auger parameter values listed in table 6 have very good correlation with theirs. From these results, we find that there are only 4-fold coordinated polyhedra in

**Table 6 Comparison of Auger parameter of present work with other works**

Samples	$\text{Al}^{\text{III}}/\alpha'(\text{eV})$	$\text{Al}^{\text{IV}}/\alpha'(\text{eV})$	$\text{Al}^{\text{VI}}/\alpha'(\text{eV})$	Reference:
$\beta$ -zeolite		1460.5		Remy <i>et al.</i>
$\beta$ -zeolite	1459.2	1460.7	1461.4	Remy <i>et al.</i>
$\beta$ -zeolite	1458.3	1460.3	1461.1	Remy <i>et al.</i>
ZM760	1458.7	1459.8	1460.9	Collignon <i>et al.</i>
NaY- zeolite		1460.6		This work

SrNaY-zeolite (ambient)		1460.1		This work
SrNaY-zeolite (900°C, 30min.)	1458.1	1459.2	1460.9	This work

zeolite-NaY and zeolite-SrNaY at room temperature. This suggests the loading of strontium ions has no apparent effect on the structure of zeolite-NaY at this stage. For the heat-treated zeolite-SrNaY, tricoodinated aluminum polyhedra exist besides tetrahedral aluminum.

### 3.2 XAS study

XAS experiments were performed to determine the impact of heat treatment at three different temperatures: room temperature (RT), 500 °C and 900 °C on the near coordination environment of Sr and Cs exchanged zeolite. Previous X-ray diffraction (XRD) work has indicated that at temperatures above 900 °C, the zeolite structure is completely destroyed through a dehydroxylation amorphization process (Gu *et al.*, 2002). However, below this temperature, the zeolite structure is retained although XRD peaks are lower in intensity. Hence, the three temperatures provided an opportunity to determine the impacts of thermal treatment on the near coordination environment above and below amorphization.

XAS can be used to characterize the near coordination environment (within 6Å) surrounding an element by providing bond distances and coordination numbers of neighboring atoms within this distance. The structural information results from analysis of the photoelectric production from the interaction of x-rays and the element under excitation. Both XANES (x-ray absorption near edge structure) and EXAFS (extended x-ray absorption fine structure) analysis are reported in this feasibility study.

Sr K-edge and Cs L-III edge x-ray absorption spectra were collected at the Stanford Synchrotron Radiation Laboratory (SSRL) using wiggler beam line 4-3 with Si(220) monochromators, beam energy 3.0 GeV, and beam current ranging from 50 to 100 mA. Spectra were collected in fluorescence mode for all samples using a 13-element Ge array detector interfaced to a multichannel analyzer. The monochromator was detuned 70% at the highest energy of the scan in order to minimize contributions from higher-order harmonics. Beam energy was calibrated by assigning the first inflection point on the absorption edge of Bi foil to energy of 16388 eV for Sr samples and the absorption edge of Ti foil to 4966 eV for Cs samples. Multiple scans (4 to 12) were collected to obtain a signal-to-noise ratio sufficiently high for extended x-ray absorption fine structure (EXAFS) analysis.

EXAFS analysis was performed for Sr using the EXAFSPAK software (George and Pickering, 1995) and the following procedure. Acceptable spectra were averaged and the background absorption was subtracted by a straight line through the pre-edge region and a three-segment spline fit in the region above the edge. The background-subtracted spectra were normalized using a Victoreen polynomial and tabulated McMaster atomic absorption fall-off coefficients. The spectra were then converted from energy to frequency space using the photoelectron wave factor,  $k$  (Brown et al., 1988; Teo, 1986). The normalized, background-subtracted,  $k^3$ -weighted XAFS spectra for reference compounds and the sorption samples were filtered over similar  $k$  ranges and Fourier-transformed with an unsmoothed window to obtain the radial structure functions (RSFs). Individual major peaks in the Fourier transform were back transformed to produce

filtered XAFS in order to isolate individual shell contributions to the XAFS (Brown *et al.*, 1988; Sayers and Bunker, 1988). Least-squares fitting of each shell was performed to determine the coordination number (CN) and bonding distance ( $R$ ). The Debye-Waller factor,  $\sigma^2$ , and  $E_0$  (defined as the energy at which  $k=0$ ), were allowed to vary during this optimization. The phase and amplitude parameters needed for the fitting were obtained from theoretical calculation results using FEFF 8.0 (Ankudinov *et al.*, 1998). Based on this fitting procedure, the resulting CN and  $R$ , were expected to be accurate to  $\pm 20\%$  and  $\pm 0.02$  Å, respectively, for the first shell (Brown, 1990). In the case of Cs, a crystal glitch for the Si(220) monochromator crystals in the EXAFS region precluded performing a detailed EXAFS analysis.

X-ray absorption near edge structure (XANES) analysis was conducted for both Sr and Cs. For this purpose, the XANES spectra were normalized to the average absorption at higher  $k$  range ( $k=3-12$ ) to allow different samples to be compared over the same scale. First derivative plots of the XANES of model compounds and samples were taken from the normalized XANES spectra; the Golay-Savitzky method was used to smooth the derivative data (Chapra and Canale, 1988). Comparison of the first derivative features provides a basis for distinguishing similarity and discrepancy in the first-shell coordination environment (Brown, 1990).

**Table 7. EXAFS fit results for Sr sorbed on zeolite before and after heat-treatment**

Sample	Sr-Z <sup>a</sup>	CN <sup>b</sup>	$R$ <sup>c</sup>	$\sigma^2$ <sup>d</sup>	$\Delta E_0$ <sup>e</sup>	
<b>SrCl<sub>2</sub>(aq)</b>	Sr-O	8.699	2.58	0.01331	-5.927	0.01M SrCl <sub>2</sub> solution
<b>Sr_2_rt</b>	Sr-O	8.923	2.57	0.01331	-8.639	Sr-zeolite, 0.2M Sr RT
	Sr-Sr	3.063	3.86	0.01678		
<b>Sr_2_500</b>	Sr-O	8.654	2.57	0.01331	-7.272	Sr-zeolite, 0.2M Sr 500°C
	Sr-Si/Al	0.974	3.38	0.00550		
<b>Sr_2_900</b>	Sr-O	7.581	2.54	0.01331	-10.384	Sr-zeolite, 0.2M Sr 900°C
	Sr-Si/Al	1.466	3.37	0.01239		
	Sr-Si/Al	1.566	3.78	0.01239		
<b>Sr_05_rt</b>	Sr-O	9.582	2.56	0.01331	-8.592	Sr-zeolite, 0.05M Sr
<b>Sr_05_500</b>	Sr-O	8.515	2.55	0.01331	-9.399	Sr-zeolite, 0.05M Sr 500°C
	Sr-Si/Al	2.118	3.38	0.01297		
<b>Sr_05_900</b>	Sr-O	6.245	2.54	0.01331	-7.434	Sr-zeolite, 0.05M Sr 900°C
	Sr-Si/Al	2.106	3.35	0.01171		
	Sr-Si/Al	0.660	3.73	0.01171		

<sup>a</sup> Z = backscatterer; <sup>b</sup> CN = coordination number; <sup>c</sup>  $R$  = interatomic distance; <sup>d</sup>  $\sigma^2$  = Debye-Waller factor; <sup>e</sup>  $E_0$  = Energy at  $k = 0$

Results of the EXAFS analysis of the Sr exchanged zeolite samples and a model aqueous Sr solution are presented in Table 7. The EXAFS spectra and the corresponding radial structure functions (RSFs) are shown in Figure 24. These data show, that for the RT samples, at both the 0.2 and 0.05 M loading conditions, exchanged Sr is very similar in structure to aqueous Sr (e.g., compare the Sr-O distances and coordination numbers (CN)

in Table 7). As indicated, the Sr-O CN is near 9 and bonding distances at 2.57 Å for both the RT samples and the aqueous Sr samples. This is expected at RT in that an

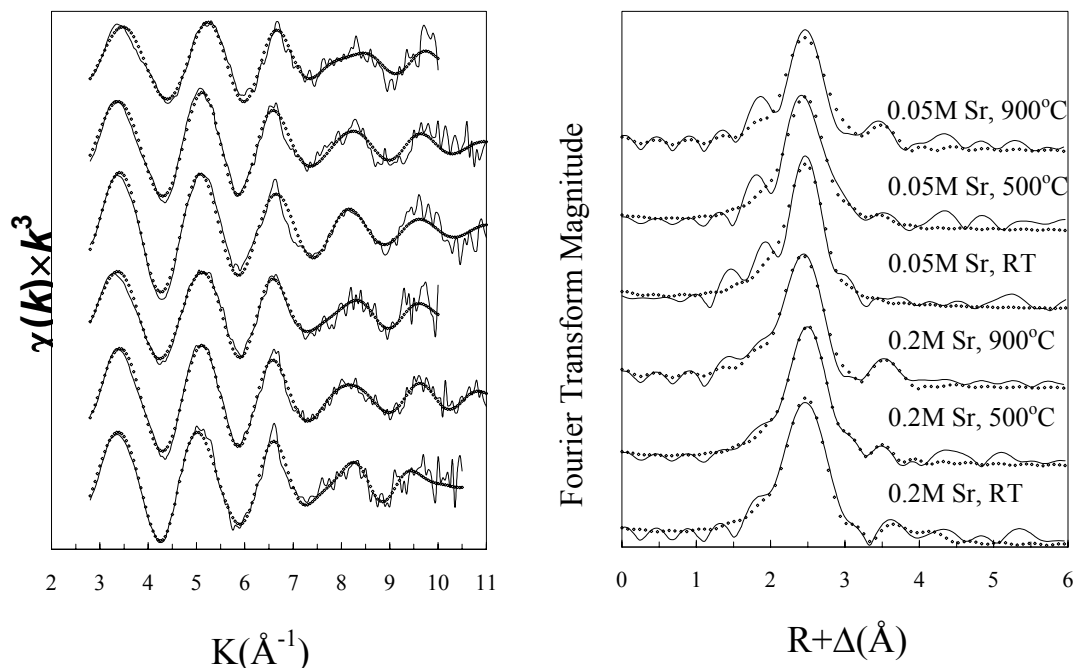


Fig. 24 Normalized EXAFS spectra and RSFs of Sr-zeolite after heat-treatment. Solid lines, experimental data; dotted lines, nonlinear least squares fit (Table 7).

outer-sphere association is expected for Sr with waters of hydration retained by Sr in supercage structure where Sr is expected to reside. A Sr-Si/Al feature is found for the heat treated samples where collapse of the supercage structure of zeolite NaY is suspected and the possible the proximity of Si/Al in the near coordination environment is consistent with such a collapse. Based on leaching studies, a recent report by Gu *et al.* (Gu *et al.* 2002) on radiation damaged zeolite NaSrY indicated that Al is leached from the zeolite structure while leaving structural Si in place in the collapsed structure.

For the heat treated samples two trends seem apparent from this initial study: (1) a consistent Sr-O distance but lower CN from heat treatment, and (2) a shorter and more obvious Sr-Si/Al neighbor for the heat treated samples compared to the RT samples. Both of these results support the idea that the near coordination environment of exchanged Sr is changing upon heat treatment and amorphizing the sample, and that the environment is more restrictive (shorter Sr-Si/Al distances with fewer waters of hydration), consistent with a collapsed of the supercage structure in which the Sr ion is exchanged.

X-ray absorption near edge structure of (XANES) analysis of the Sr XAS also indicates that heat treatment affects the near coordination environment of Sr (Figure 25a). A first derivative plot (Figure 25b) of the XANES shows different locations for peak features, strong evidence of different near coordination environment among the different loading conditions and heat treatment. More loading conditions and heat treatment XAS

data need to be collected to further substantiate the cause and effect to the XANES attributes. Nonetheless, the fact that differences are noticeable is strong evidence of a clear heat treatment effect. XANES and first derivative plots of heat treated and untreated Cs exchanged zeolite are shown in Figure 26a and 26b, respectively.

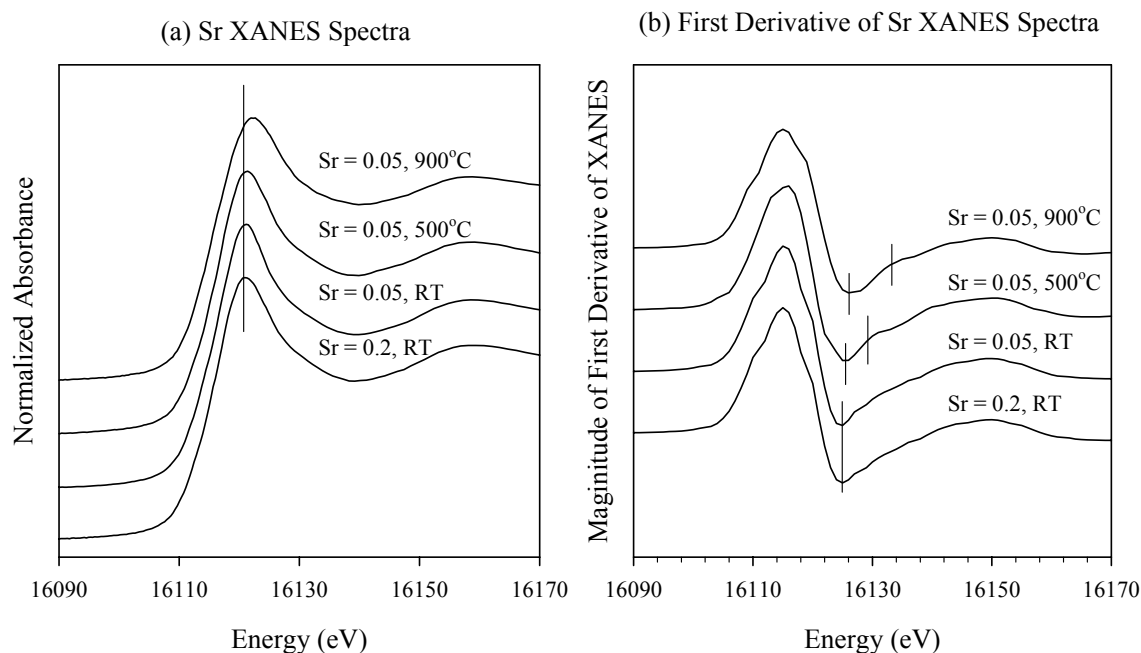


Fig. 25 (a) Normalized XANES spectra and (b) first derivative of XANES spectra of strontium in zeolites. Vertical bars represent the different features shown on the spectra between samples.

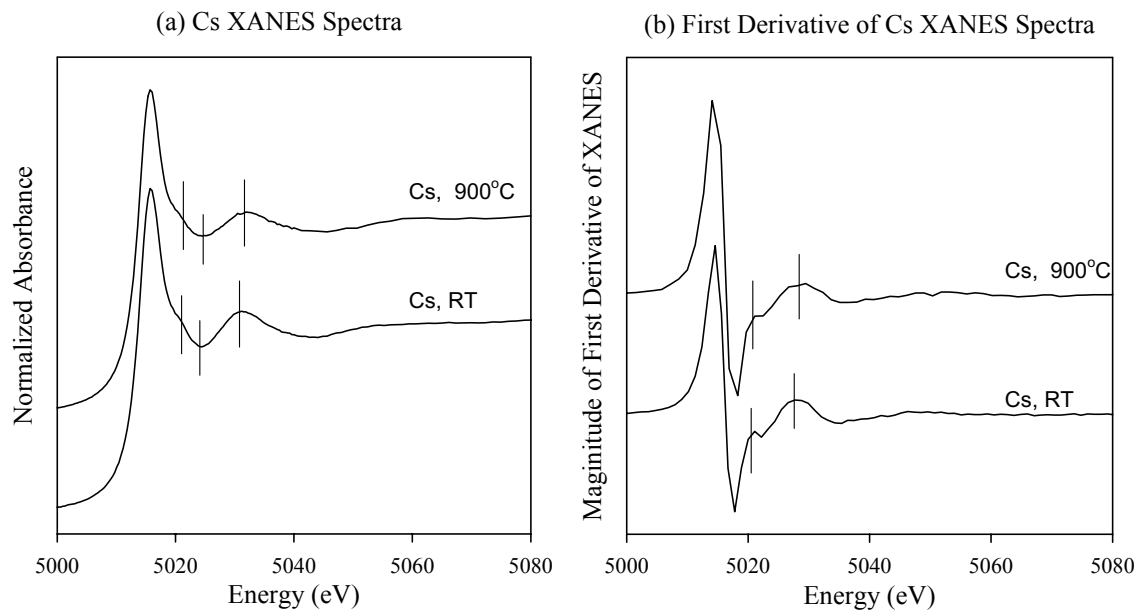


Fig. 26 (a) Normalized XANES spectra and (b) first derivative of XANES spectra of cesium in zeolites. Vertical bars represent the different features shown on the spectra between samples.



Although the exact basis for the features is not known at this time, the clear difference between the treated and untreated samples indicates a very different near coordination environment for the two samples. Further EXAFS and XANES analyses will be needed to further clarify the basis for these differences for Sr and Cs.

#### 4. Thermal effects on the Sr sorption on clay

Strontium sorption experiments were performed on heated clay minerals as part of an effort to investigate the impact of heating on the sorption properties of these common geosorbents used in barrier and binder applications. The local coordination environment of Sr sorbed on montmorillonite before and after thermal-treatment was characterized using XAS. Heat-treatment was performed either before or after the Sr-loading. Heating was originally proposed as a convenient and efficient alternative for the irradiation of minerals. It was expected that heat treatment simulates the impact of ionizing radiation on the mineralogical and sorptive properties of clay minerals at least to the extent that amorphization is the primary damage result. Heating also has relevance to the nuclear waste disposal in that many of the potential nuclear waste repositories have undergone or may experience various thermal events.

Cheto montmorillonite (SAz-1) from Arizona and kaolinite (KGa-1) from Georgia were supplied from the Source Clays Repository of the Mineralogical Society of America. The clay samples were pretreated to remove organic and inorganic impurities following the procedure described in detail in Morton et al. (2001).

Heating was performed at various temperatures using an automated programmable electrical furnace (Lindberg Blue). Heating at 900°C for 30 minutes was selected to simulate the amorphization caused by ionizing radiation based on our previous research (Gu, 2001). The temperature was increased at the rate of 20°C/min. The montmorillonite and kaolinite heated at 900°C for 30 minutes were fully amorphized and no new high temperature phase formed as is confirmed by XRD. The heat-treatment of Sr-preloaded clay minerals was performed at the same conditions following the same procedure.

$10^{-4}$ M Sr was adsorbed on montmorillonite and kaolinite before and

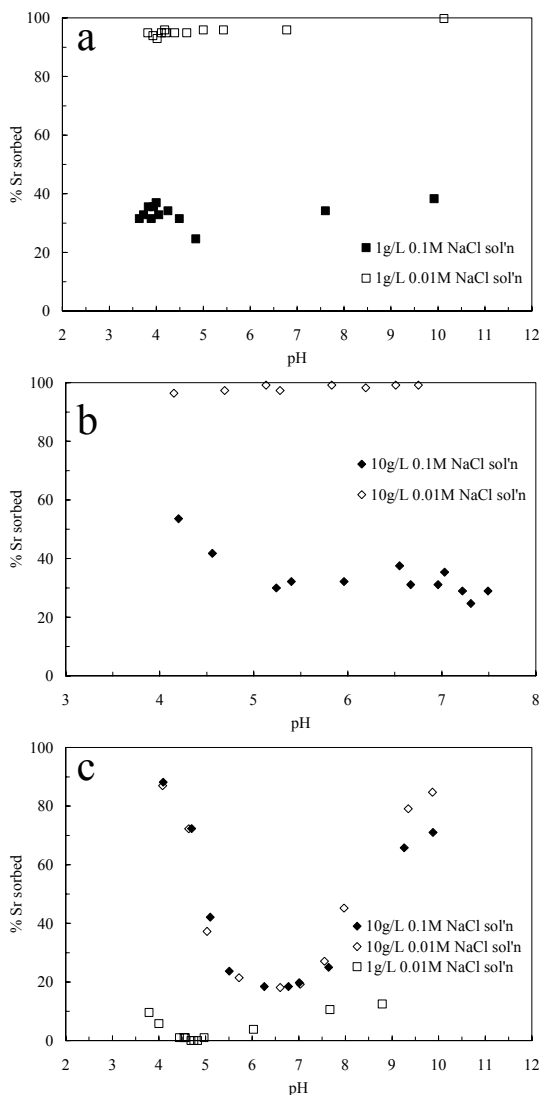


Fig. 27 Sr-sorption on montmorillonite a) before heat-treatment and after heat-treatment at b) 400°C for an hour and c) 900°C for 30 minutes.

after heat-treatment. 100mg or 10mg clay was reacted with 10ml of background electrolyte solution containing Sr. The ionic strength of the suspension was adjusted using an ACS grade NaCl (Fisher Chemical) to 0.1 or 0.01 M. The pH of the suspension was adjusted using a 1N NaOH or HCl volumetric standard solution (Fisher Chemical). All solutions were prepared using ultrapure water (18M $\Omega$ -cm, MilliQ-water system). The suspension was continuously shaken using an end-over-end shaker at room temperature and allowed to reach equilibrium in a tightly capped 15ml polypropylene centrifuge tube. After 5 days of equilibration period, the final pH of the suspension was measured (Orion 520 pH-meter and Ross Combination Electrode) and the solid phase was separated from the solution by centrifugation at 6000 rpm for 30 minutes. The final Sr concentration in solution was measured using an atomic absorption spectrometer (GBC 903). The solid was used for Sr XAS study.

Sr sorption on montmorillonite showed no distinct dependency on the solution pH (Figure 27a). As an alkaline earth element, the driving force for the adsorption of Sr to montmorillonite is expected to be the electrostatic attraction due to the net negative charge at the surface originating from the isomorphous substitution in the structure. This structural charge is independent of the pH of the bathing solution. Therefore, the Sr sorption is pH-independent. However, this weak electrostatic nature of sorption makes the amount of sorbed Sr strongly dependent on the Na<sup>+</sup> concentration that can effectively compete with Sr<sup>2+</sup> for cation exchange sites. Montmorillonite heated at 400°C shows similar Sr sorption behavior to that of unheated montmorillonite (Figure 27b). The maintenance of the sorption property suggests that the montmorillonite structure is retained after 400°C heating. The XRD also confirms the maintenance of the montmorillonite structure (Gu *et al.*, 2001) at this temperature. 900°C-heated montmorillonite, however, shows different sorption properties (Figure 27c). At this temperature amorphization results and the layer structure of montmorillonite collapses through complete dehydroxylation.

We also performed Sr sorption montmorillonite samples that had been amorphized 900°C. Sr sorption to this surface as a function of pH has a U-shaped sorption curve. The minimum amount sorbed at near neutral pH and increase in sorption with decreasing pH at acidic pH conditions are quite different than that expected for ordinary sorption behavior of metal cations on aluminosilicates in which uptake is either independent of pH (Figure 27a) or increasing with pH like that shown in the high pH region when sorption is predominantly at edge sites. One possible reason for the unusual behavior at low pH is that referential leaching of aluminum from the montmorillonite occurs at these low pH conditions for samples that have been amorphized. This might have left the remaining structure with positive charge deficiency and very reactive to the positively charged Sr<sup>2+</sup>. Another possibility is the coprecipitation of Sr ions with some dissolved Al in a strontium aluminate solid, although we have not found any reports of such a phase in the literature to date. For now, it is not possible to determine which one is the actual mechanism. More study is needed for a more precise characterization of the sorption mechanism at low pH.

Sorption capacity of kaolinite for Sr is much lower than that of montmorillonite as expected from the surface area and surface charge consideration. The sorption data are quite scattered and the sorption is almost pH-independent but is strongly dependent on the Na<sup>+</sup> concentration under the experimental condition (Figure not shown). The Sr sorption on 900°C-heated kaolinite is very similar to that on 900°C-heated

montmorillonite. This similarity suggests the possibility of the formation of similar amorphized material from both minerals upon heating at 900°C.

XAS studies were performed on the untreated and heat treated Sr loaded clay samples. The Sr sorbed on unheated montmorillonite has an EXAFS spectrum similar to that of fully hydrated aqueous  $\text{Sr}^{2+}$  ions (Table 8). Regardless of sorption pH (4.1 or 6.7), outer-sphere complex is formed at the interlayer or edge surface, retaining its first hydration sphere upon adsorption (CN=9.2-9.4, R=2.57-2.58Å). The

**Table 8 EXAFS fit results for Sr sorbed on montmorillonite before and after heat-treatment**

Sample	Sr-Z	CN	R	$\sigma^2$	$\Delta E_0$	
Mtun_4_rt	Sr-O	9.222	2.58	0.01331	-5.608	Sr-montmorillonite PH=4.1, RT
Mtun_4_400	Sr-O	7.859	2.57	0.01331	-7.459	Sr-montmorillonite pH=4.1, 400°C
Mtun_4_900	Sr-O	4.458	2.54	0.01331	-7.734	Sr-montmorillonite pH=4.1, 900°C
	Sr-Si/Al	2.034	3.28	0.01425		
	Sr-Si/Al	1.499	3.76	0.01425		
Mtun_7_rt	Sr-O	9.401	2.57	0.01331	-6.164	Sr-montmorillonite PH=6.7, RT
Mtun_7_900	Sr-O	4.676	2.53	0.01331	-7.411	Sr-montmorillonite pH=6.7, 900°C
	Sr-Si/Al	1.591	3.27	0.01275		
	Sr-Si/Al	1.432	3.76	0.01275		
Mt400_4_rt	Sr-O	9.004	2.58	0.01331	-5.807	Sr on 400°C heated montmorillonite, pH=4.1
Mt900_10_rt	Sr-O	9.287	2.57	0.01331	-7.789	Sr on 900°C heated montmorillonite, pH=9.8
	Sr-Sr	1.872	3.49	0.02017		

Sr-montmorillonite heated at 400°C has almost the same EXAFS parameters as untreated except a slight decrease in coordination number of 7.9 is noted. This means that heating to this temperature does not cause a full structural change, so that the mineral retains its specific sorption property. Sr on preheated montmorillonites, either at 400°C or 900°C, apparently forms an outer-sphere complex similar to that on unheated montmorillonite as evidenced by the similarities of the CN and R distances of sorbed Sr and aqueous Sr (Table 8, Figure not shown). However, the Sr-montmorillonite heated at 900°C has a different local coordination environment characterized by a low coordination number for the first shell of oxygens (4.5-4.7) and shorter bond length (2.53-2.54 Å) between Sr and nearest neighbor O atoms. Sr in these samples also shows the Si/Al neighbors.

These results show that the outer-sphere coordinated Sr, either in the interlayer or at surfaces edges at room temperature, migrates into the lattice structure upon heating at 900°C and becomes incorporated into a newly formed amorphous structure. However, no Sr neighbors were observed in the local environment of Sr. This means that the adsorbed Sr ions do not form a Sr-mineral upon heating. Instead, they are scattered more uniformly over the newly formed amorphous phase.

## **Publications and invited presentations:**

### ***(A) Papers published in refereed research journals or conference proceedings:***

1. L.M. Wang, S.X. Wang, W.L. Gong and R.C. Ewing, "Temperature dependence of Kr ion-induced amorphization of mica minerals", *Nuclear Instruments and Methods in Physics Research B* 141 (1998) 501-508.
2. L.M. Wang, "Application of advanced transmission electron microscopy techniques in the study of radiation effects in insulators", *Nuclear Instruments and Methods in Physics Research B* 141 (1998) 312-325.
3. L.M. Wang, S.X. Wang and R.C. Ewing, "Radiation effects in zeolite: Relevance to near-field containment", Proceedings of the 9th Annual International High-Level Radioactive Waste Management Conference (American Nuclear Society, Las Vegas, NV, May 11-14, 1998), pp. 772-774.
4. L.M. Wang and R.C. Ewing, "Transmission electron microscopy study of radiation effects in materials for nuclear waste disposal", *Electron Microscopy 1998*, Proceedings of the 14<sup>th</sup> International Congress on Electron Microscopy (Cancun, Mexico, Aug 31-Sept. 4, 1998), Edited by H.A. Calderón Benavides and M. José Yacamán, Vol. 2, 825-826.
5. S.X. Wang, L.M. Wang and R.C. Ewing, "Electron irradiation of zeolites", *Materials Research Society Symposia Proceedings* 540 (1999) 361-366.
6. B.X. Gu, S.X. Wang, L.M. Wang, and R.C. Ewing, "Radiation and thermal effects on the structure and ion-exchange/retention capacity of zeolites", *Proceedings of the International Conference on the Future Nuclear Systems—Global'99* (American Nuclear Society, Jackson Hole, Wyoming, August 29-September 3, 1999).
7. L.M. Wang, S.X. Wang, W.L. Gong, R.C. Ewing and W.J. Weber, "Amorphization of ceramic materials by ion beam irradiation", *Materials Science & Engineering A* 253 (1998) 106-113.
8. B.X. Gu, L.M. Wang and R.C. Ewing, "The effect of amorphization on the Cs ion exchange and retention capacity of zeolite-NaY", *Journal of Nuclear Materials* 278 (2000) 64-72.
9. S.X. Wang, L.M. Wang and R.C. Ewing, "Electron and ion irradiation of zeolites", *Journal of Nuclear Materials* 278 (2000) 233-241.
10. Binxi Gu, Lumin Wang, Phil A. Simpson, Leah D. Minc and R.C. Ewing, "Radiation and thermal effects in zeolite-NaY", in: *Scientific Basis for Nuclear Waste Management XXIII*, R.W. Smith and D.W. Shoesmith eds. (Material Research Society, Warrendale, PA, 2000), 493-498.
11. B.X. Gu, L.M. Wang, S.X. Wang, D.G. Zhao, V.H. Rotberg and R.C. Ewing, The effect of H<sup>+</sup> irradiation on the Cs ion exchange capacity of zeolite-NaY, *J. Materials Chemistry* 10 (2000) 2610-2616.
12. M. Nyman, B.X. Gu, L.M. Wang, R.C. Ewing and T.M. Neoff, Synthesis and characterization of a new microporous cesium silicotitanate (SNL-B) molecular sieve, *Microporous Materials* 40 (2000) 115-125.
13. M. Nyman, F. Bonhomme, D.M. Teter, R.S. Maxwell, B.X. Gu, L.M. Wang, R.C. Ewing and T.M. Neoff, Integrated experimental and computational methods for structure determination and characterization of a new, highly stable cesium silicotitanate phase, Cs<sub>2</sub>TiSi<sub>6</sub>O<sub>15</sub> (SNL-A), *Chemistry of Materials* 12 (2000) 3449-3458.
14. L.M. Wang, B.X. Gu, S.X. Wang and R.C. Ewing, "Radiation effects on materials in the near-field of a nuclear waste repository", in: *Scientific Basis for Nuclear Waste*

- Management XXIV*, K.P. Hart and G.R. Lumpkin eds. (Material Research Society, Warrendale, PA, 2001), 883-891.
15. B.X. Gu, S.X. Wang, L.M. Wang and R.C. Ewing, "The effects of proton beam irradiation on the Cs ion exchange capacity of zeolite-NaY", *Journal of Nuclear Materials*, in preparation.
  16. Binxi Gu, Lumin Wang, Shixin Wang, Donggao Zhao, Victor H. Rotberg, R.C. Ewing, Effects of proton irradiation in zeolite-Y, *Materials Research Society Symposia Proceedings* 650 (2001) R3.16.1-6.
  17. B.X. Gu, L.M. Wang, L.D. Minc and R.C. Ewing, Temperature effects on the radiation stability and ion exchange capacity of smectites, *J. Nuclear Materials* 297 (3) (2001) 345-354.
  18. B.X. Gu, L.M. Wang and R.C. Ewing, Radiation effects on the microstructure and chemical properties of zeolite-Y, *Transactions of the American Nuclear Society* 84 (American Nuclear Society, Chicago, IL, 2001), pp. 358-359.
  19. B. Gu, L. Wang and R.C. Ewing, The effects of radiation on the retention of strontium in zeolite-NaSrY, *J. Materials Chemistry* 12 (2002) 233-238.
  20. J. Chen, L.W. Beck, L.M. Wang, B.X. Gu, and R.C. Ewing, MAS NMR Study on the Microstructural Changes of Zeolite-NaY Under Neutron Irradiation. In Radiation Effects and Ion Beam Modification of Materials, L.M. Wang, R. Fromknecht, L.L. Snead, D.F. Downey, H. Takahashi (Eds.), Proceedings of the Materials Research Society 792 (2004) 417-422.
  21. J. Chen, L. M. Wang, L. W. Beck, B. X. Gu, R. C. Ewing, L. Minc, "MAS NMR Study on the Microstructure Evolution of Zeolite under Neutron Irradiation", *Journal of Applied Physics* (to be submitted).
  22. J. Chen, S. P. Hyun, L. M. Wang, L. W. Beck, K. F. Hayes, R. C. Ewing, "Influence of Neutron Irradiation on the Structure of Strontium-loaded Zeolite: MAS NMR and XANES Investigation", *Journal of Material Chemistry* (to be submitted).
  23. B. X. Gu, J. Chen, L. M. Wang, R. C. Ewing, X-Ray Photoelectron Spectroscopy Study of Radiation and Thermally-Induced Amorphization In Zeolite-NaY, *Journal of Material Chemistry* (to be submitted).
  24. S.P. Hyun, L.M. Wang, and K.F. Hayes, XAS study of the impact of thermal treatment of Sr coordination by zeolite-NaY (in preparation).
  25. S.P. Hyun, L.M. Wang, and K.F. Hayes, XAS study of the impact of neutron irradiation on Sr coordination by zeolite-NaY (in preparation).
  26. S.P. Hyun and K.F. Hayes, XAS study of Sr sorption and exchange behavior on heat treated clays (in preparation).

**(B) Ph.D. Thesis completed:**

Binxi Gu, "Radiation and Thermal Effects on Zeolites, Smectites and Crystalline Silicotitanates", *University of Michigan*, Ann Arbor, Michigan (2001).

**(c) Invited Talks:**

1. L.M. Wang, "Radiation Effects in Nuclear Waste materials and Their Consequences", at International Conference on Applied Mineralogy (ICAM) 2000 at Gottingen, Germany (July 19, 2000).

2. L.M. Wang, "Radiation effects in complex ceramic materials": at the Institute of Transuranium Elements, European Commission Joint Research Center, Karlsruhe, Germany (July 31, 2000).
3. L.M. Wang, "Radiation effects in nuclear waste materials and their consequences": at the TMS (The Minerals, Metals and Materials Society) 2000 Fall Meeting, St. Louis, MO, (October 9, 2000).
4. L.M. Wang, "Nuclear waste forms for the future": at the 221st National Meeting of the American Chemical Society, San Diego, CA (April 1-5, 2001).
5. L.M. Wang, "TEM study of radiation effects in solids", "Effects of ionizing irradiation on the structure and ion exchange capacity of zeolite and clays": at Laboratory of Mineralogy and Crystallography, Paris University VI & VII, Paris, France (September 18, 2001).
6. L.M. Wang, "In situ TEM study of radiation effects in nuclear ceramics": at International Conference on Modern Materials and Technologies, the 10<sup>th</sup> International Ceramic Congress and the 3<sup>rd</sup> Forum on New Materials, Florence, Italy (July 17, 2002).
7. L.M. Wang, "Radiation effects in nuclear waste glasses": at the Symposium on Microstructural Processes in Irradiated Materials (TMS 2003 Spring Meeting), San Diego, California (March 3-6, 2003).
8. L.M. Wang, "Radiation effects in zeolites and clays for the sorption and release of radionuclides during transport through the geosphere": at the Environmental Management Science Program (EMSP) Symposium on Nuclear Waste Management, the 226th American Chemical Society National Meeting, NYC, NY (September 7-11, 2003).
9. L.M. Wang, "Radiation Effects in Apatite Materials": at the Center for Advanced Research of Ecomaterials, Institute of Environmental Science and Engineering, Nanyang Technological University, Singapore (February 25, 2004).
10. L.M. Wang, "Radiation Effects in Ceramic Materials for the Radioactive Waste Management": at the School of Material Engineering, Nanyang Technological University, Singapore (March 17, 2004).

## REFERENCES

- Ali, S., A. H., Hassan, N. A. *et al.*, (1994), *J. Radia. Nucl. Chem.*, 187, 223.
- Ankudinov, A.L., Ravel, B., Rehr, J.J., Conradson, S.D. (1998), *Phys. Rev. B*, 7565.
- Auroux, A., Huang, M., Kaliaguine, S., (1996), *Langmuir*, 12, 4803.
- Brown G. E., Jr. (1990), In *Mineral-Water Interface Geochemistry*, Vol.23, edited by M. F. Hochellar, Jr. and A. F. White, (Mineralogical Society of America) 309.
- Brown G. E., Jr., Calas, G., Waychunas G. A., Petiau J. (1988), In *Mineral-Water Interface Geochemistry*, Vol. No.18, edited by F. C. Hawthorne, (Mineralogical Society of America) 431.
- Bursill, L. A., Lodge, E. A., *et al.*, (1980), *Nature* 286, 111.
- Cambor, M. A., Hong S. B., Davis, M. (1996), *Chem. Commun.*, 425.
- Chan, S. L., Glandden, L. F., Elliott, S. R., (1988), *J. Non-Crystal. Solids*, 106, 413.
- Chapra, S. and Canale, R. (1988) *Numerical methods for engineers*. McGraw-Hill.
- Chen, C.C., Papelis, C., and Hayes, K.F. (1998) Extended X-Ray Absorption Fine Structure (EXAFS) Analysis of Aqueous Sr(II) Ion Sorption at Clay-Water Interfaces, In *Adsorption of Metals* (ed. E.A. Jenne), Chapter 15, 333-348.

- Chen, C.C and Hayes, K.F. (1999) X-ray absorption spectroscopy investigation of aqueous Co(II) and Sr(II) sorption at clay-water interfaces, *Geochem. Cosmochim. Acta*, 63, 3205-3215.
- Collignon, F., Jacobs, P. A., Grobet, P., Poncelet, G. (2001), *J. Phys. Chem.B*, 105, 6812.
- Devine R. A. B., Marchand, M. (1993), *Appl. Phys. Lett.*, 63, 619.
- Durrani, S. K., Dyer, A., Blackburn, R. (1993), *Zeolites*, 13, 2.
- Engelhardt, G., Radeglia, R. (1984), *Chem. Phys. Lett.*, 108, 271
- Flanigen, E. M.(1971), in *Zeolite Chemistry and Catalysis*, *ACS Monograph*, Vol 171, edited by J. A. Rabao (American Chemical Society) 80.
- Galeener, F. L. (1979), *Phys. Rev. B*, 19, 4292.
- Georger, A. R., Catlow, C. R. A., Thomas, J. M. (1991), *Catalysis Lett.*, 8, 193.
- George G. N. and Pickering I. J. (1995), *EXAFSPAK-A suite of computer programs for analysis of X-ray absorption spectra* (Stanford Synchrotron Radiation Laboratory).
- Gu, B.X., Wang, L.M. and Ewing, R.C. (1999), *J. of Nucl. Mater.* , 278, 64.
- Gu, B., Wang, L., and Ewing, R.C. (2002), *J. Mater. Chem.*, 12, 233.
- Gu, B. (2001), Ph.D. Dissertation, University of Michigan.
- Gu, B., Wang, L., and Ewing, R.C. (2002), *J. Mater. Chem.*, 12, 233.
- Hong, S. B., Camblor, M. A., Davis, M. E. (1997), *J. Am. Chem. Soc.*, 119, 761.
- Hosono, H (1991), *J. Appl. Phys.*, 69, 8079.
- Huang, Y. N. (1998), *J. Mater. Chem.*, 8, 1067.
- Huang, Y. N, Havenga, E. A. (2001), *Chem. Phys. Lett.*, 345, 65.
- Lippmaa, E and Magi, M. (1986), *J. Am. Chem. Soc.*, 108, 1730.
- Loewenstein W. (1954), *Am. Mineral*, 39, 92.
- Morton, J.D., Semrau, J.D., and Hayes, K.F. (2001), *Geoch. et Cosm.* 65, 2709.
- Norby, P, Poshni, f. I. (1998), *J. Phys. Chem.*, 102, 839.
- Naguib, H., M., Kelly, R. (1975), *Rad. Effects* 25, 1
- Primak, W, Edwards, E, *et al.* (1964), *Phy. Rev.*, 113, A531.
- Qin, L. C., Hobbs, L. W. (1995), *J. Non-Cryst. Solids* 192 & 193, 456.
- Radeglia, R., Engelhardt, G. (1985), *Chem. Phys. Lett.*, 114, 28.
- Ramdas, S., Klinowski, J., (1984), *Nature*, 308, 521.
- Remy, M. J., Genet, M. J., Notte, et al. (1993), *Micr. Mater.*, 2, 7.
- Sayers D. E. and Bunker B. A. (1988), In *X-ray Absorption: Principles, Applications, Techniques of EXAFS, SEXAFS and XANES*, Vol. 92, edited by D. C. Koningsberger and R. Prins (John Wiley & Sons) 211.
- Selim, M., M., Kira, A. I. (1992), *J. Radia. Nucl. Chem.*, 164, 229.
- Sen, P. N. and Thorpe, M. F. (1977), *Phys. Rev. B*, 15, 4030.
- Smith, J. V. and Blackwell, C. S. (1983), *Nature*, 303, 223.
- Stubican, V., Roy, R. (1961), *Amer. Min.* 46, 32.
- Szostak, R., Thomas, T. L. (1986), *J. Catal.* 101, 549.
- Teo, B. K. (1986), *EXAFS: Basic Principles and Data Analysis* (Springer-Verlag).
- Thomas, J. M., Fyfe, C. A., *et al.* (1982), *J. Phys. Chem.*, 86, 3061.
- Thomas, J. M., Klinowski, J., *et al.* (1983), *Chem. Phys. Lett.*, 102, 158.
- Treacy, M., M., J., Newsam, J., M. (1987), *Ultramicroscopy*, 23, 411.
- Wang, L.M., Wang, S.X. and Ewing, R.C. (1998), *Proceedings of the 9th Annual International High-Level Radioactive Waste Management Conference* (American Nuclear Society, Las Vegas, NV, May 11-14, 1998) 772.

- Wang, L.M., Wang,S.X., Gong, W.L., Ewing, R.C. and Weber, W.J. (1998), Mater. Sci.& Engin. A 253, 106.
- Wang, L.M., Weber, W.J. (1999), Phil. Mag. A, 237.
- Wang, S.X., Wang, L.M and Ewing, R.C. (2000), J. Nucl. Mater., 278, 233.
- Wright, A. C., Bachra, B., Brunier, T. M., *et al.* (1992), J. Non-Crystal., 150, 69.



## **PROPOSED FUTURE RESEARCH**

At this stage, we have to admit that our research program is still incomplete. Extended duration and increased funds are needed to complete all the tasks specified in our original proposal mainly because of the following facts: (1) The lower than expected neutron flux in the reactor has caused a longer time needed for achieving the radiation dose required for amorphizing the zeolite samples. (2) The unexpected levels of radioactivity of the neutron irradiated samples (especially with Sr and Cs loadings) due to trace amount impurities have caused extensive extra work for handling and analyzing these samples safely. Although neutron irradiation of twenty four zeolite samples (eight loaded with Sr and another eight loaded with Cs) have been completed, several the Sr loaded samples and all of the Cs loaded samples became highly radioactive after neutron irradiation. It took a long time for us to get permission on the handling the Sr loaded samples with several revisions of processing methods for ion exchange/leaching and analytical work since every step was checked very strictly by the health physicist from OSEH. All of the Cs loaded samples showed >1.5 R/hr radioactivity and they have to be processed in the hot cell in the Phoenix Memorial Laboratory in our university by specially trained staff. In addition, we have also finally obtained a special permission from the Stanford Synchrotron Radiation Laboratory for conducting X-ray absorption spectroscopy studies on some of the radioactive samples.

The following are some of our proposed future research topics:

1. Desorption and leaching test of neutron irradiated strontium and cesium loaded zeolite (zeolite-SrNaY and zeolite CsNaY)

The desorption of strontium and cesium from the neutron irradiated zeolites as well as the leaching behavior of the radiation damaged zeolite are very important issues specified in our previous research proposal. This work is the continuation of the previous project. Since the samples are radioactive (especially the Cs loaded samples), most of these experiments will be conducted in the hotcell at the Phoenix Memorial Laboratory of the University of Michigan with the support of skilled laboratory staff. Some strontium loaded samples will be processed in a glove box instead of a hotcell with the procedures that have already been approved by radiation safety personnel.

2. *In-situ* XPS research on argon and electron irradiated zeolites

The X-ray photoelectron spectrum (XPS) analysis and magic angle spinning nuclear magnetic resonance (MAS NMR) are the two methods to directly relevant to chemical bonding for both crystalline and amorphous solid among the methods employed in the zeolite research. In the case of research of the ion irradiation effects on complex ceramics, it is very difficult to get a bulk irradiated sample due to the limitation of the depth of irradiated ions, which is the essential requirement for MAS NMR. XPS is a surface sensitive analysis method. Its analysis depth overlaps those of irradiated materials makes XPS is a very suitable characterization method for the irradiation effects on solids. However, that the perturbing the surface properties or contamination during the transfer of the samples after irradiation could complicate or mislead the XPS indication. Thus, XPS characterization on *in-situ* ion irradiation of zeolites is very important to reveal the real changes of the microstructure. For this planed *in-situ* XPS work, electron and

neutron argon irradiation can be conducted in the chamber of XPS instrument. This can make the surface of zeolites free from contamination. And, most importantly, the microstructure changes of zeolite with various dose level can be studied in details.

### 3. IR experiment on neutron-irradiated zeolites

Detailed MAS NMR work has already been conducted on neutron-irradiated zeolites. We found that the decrease of the Si-O-T bond angle occurred in the structure. IR analysis, however, can yield information not only on short range bond order and characteristics but also on long range order. Thus, combined the MAS NMR and IR together, more detailed microstructure changes can be disclosed. In this section, IR experiment will be conducted on zeolites irradiated on different dose level.

### 4. XAS Study

As the above XAS studies indicate, significant progress has been made in characterizing the changes in the local coordination environment of sorbed cations caused by thermally treated and neutron irradiated clay and zeolite samples. The highlights of the work include demonstrating for the first time that: (1) amorphization of clays and zeolites produces a “new phase” association for Sr compared to untreated and aqueous samples of Sr that exists in absence of damage, (2) that the irradiation damage results in more effectively sequestered Sr when it occurs subsequent to cation exchange, the most likely scenario at nuclear repositories, (3) that neutron bombardment damage can lead to intermediate stages of damage compared to the amorphization caused by thermal treatment, and (4) that clay minerals and zeolites can be partially amorphized by neutron damage leading to Al leaching and the formation of a new Sr/Al phases that make Sr less available than sorbed Sr to undamaged materials. While these results point to the favorable impact of radiation damage on geosorbents from a permanent sequestration viewpoint, additional work remains to more fully understand the mechanism and generality of these results to other radionuclides and irradiation damage conditions.

One key question that remains unanswered is whether the level of neutron irradiation induced damage observed in this study is an intermediate stage of damage that ultimately will lead to complete amorphization like that caused by heat treatment if sufficient exposure time or flux is allowed. Although additional samples that have been exposed to neutron damage for much longer times and at higher fluxes at the Pheonix Memorial Laboratory nuclear reactor at the University of Michigan have yet to be analyzed. A two year extension of this work with additional funds would allow us to analyze more of these “hot” samples. Another key question is whether the results for Sr are unique to that element. For example, will other radionuclides (e.g., U(VI) or Cs(I)), with different sorption behavior and affinity for clays and zeolites, give similar results to Sr? In order to answer this question and generalize these results, additional studies with these other elements will need to be conducted. Although we originally proposed to perform studies on U and Cs, we have not yet had a chance due to the limitation of access to neutron activated samples for these elements, and the unanticipated extra time, training, permission, and money needed for working with highly radioactive samples. One potential way to alleviate the bottleneck with radioactive samples is to perform studies using a suitable electron beam source that does not generate radioactive samples but which is expected to also simulate similar aspects of radiation damage compared to

neutron damage. While electron beam experiments were originally proposed, access to a suitable electron beam source with sufficient energy and surface area was ultimately not possible. Recently, however, we have identified a company (Electron Solutions, Inc, MA) with an electron beam source having sufficiently high energies (up to 5 MeV) and a surface area (2 cm<sup>2</sup> beam area) that will allow us to process our samples for a nominal fee. This should allow us to produce the necessary quantities of damaged material for a more complete study. As such, one of our proposed tasks for the two year continuation is to use this electron beam source to produce sufficient (and non-radioactive) amounts of damaged geosorbents for a more comprehensive XAS study of other elements.

Finally, having the highly rated and approved research program at SSRL (valid through 2005) affords us the unique opportunity to characterize the near coordination environment of the necessary number of samples for the next two years and to complete the original objectives of this study. With access to SSRL facilities and beamlines now secured, and experienced gained during the past two years, we are poised to answer the remaining key questions in the next two years. For us to do so, however, the additional two years of support requested from the EMSP program is essential.

The final results of this research will provide a fundamental understanding of retention or release of radionuclides from geologic materials (clays and zeolites) in the radiation-fields that are present in a variety of DOE sites, such as Hanford, INEEL and eventually at Yucca Mountain.